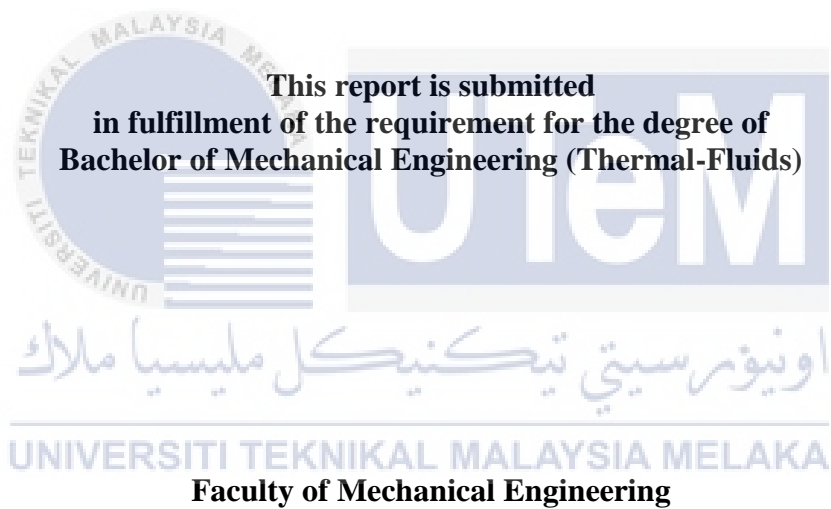


**A COUPLED SIMULATION METHOD FOR A VORTEX-INDUCED VIBRATION
SYSTEM**

MONG GUO REN



UNIVERSITI TEKNIKAL MALAYSIA MELAKA

2017

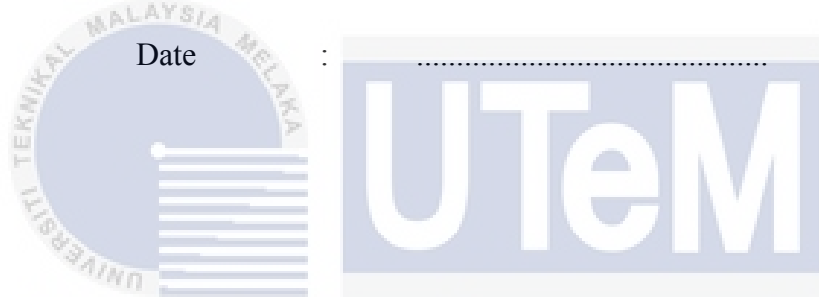
DECLARATION

I declare that this project report entitled “A Coupled Simulation Method For A Vortex-Induced Vibration System” is the result of my own work except as cited in the references

Signature :

Name :

Date :



اونيورسيتي تيكنيكل مليسيا ملاك

UNIVERSITI TEKNIKAL MALAYSIA MELAKA

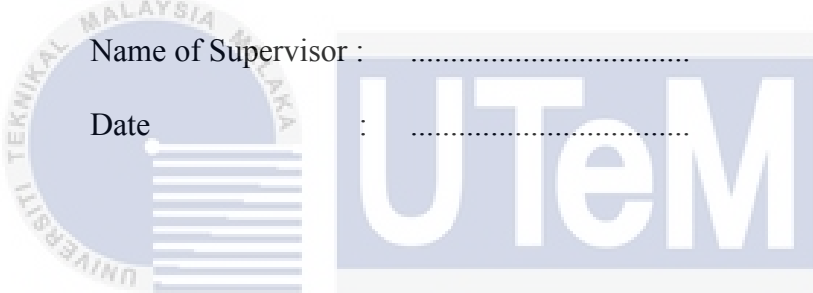
APPROVAL

I hereby declare that I have read this project report and in my opinion this report is sufficient in terms of scope and quality for the award of the degree of Bachelor of Mechanical Engineering (Thermal-Fluids).

Signature :

Name of Supervisor :

Date :



اونيورسيتي تيكنيكل مليسيا ملاك

UNIVERSITI TEKNIKAL MALAYSIA MELAKA

DEDICATION

To my beloved father and mother.



ABSTRACT

Fluid structure interaction is a phenomenon that happened around us every day. Whenever there is fluid flowing around a stationary object, fluid induced effect will occur on the object. Simulation carried out using computer aided engineering (CAE) usually does not include body motion to reduce the simulation time. This project is carried out to identify will the body motion effect on flow behaviour in high Reynolds Number. Airfoil cross-section of NACA0018 is chosen to be simulated using ANSYS Fluent v16. Fixed airfoil simulation is carried out to find the presence of vortex shedding and Strouhal Number. Two more categories of simulation is carried out using Reynolds Number of 10^5 and 10^4 . Both simulations have a system with different stiffness and natural frequency. Result shows that the Strouhal Number of vortex shed remains at 0.732 despite a change in system stiffness and Reynolds Number



ABSTRAK

Cecair interaksi struktur adalah satu fenomena yang berlaku di sekeliling kita setiap hari. Apabila terdapat cecair mengalir di sekitar objek, objek akan mengalami sejenis kesan daripada aliran cecair. Kebiasaannya simulasi yang dijalankan menggunakan komputer kejuruteraan (CAE) tidak termasuk pergerakan badan untuk mengurangkan masa penyelakuan. Projek ini dijalankan untuk mengenal pasti adakah pergerakan badan menjejaskan tindak balas badan yang disebabkan oleh aliran bendalir dalam tinggi Nombor Reynolds. Keratan rentas aerofoil NACA0018 dipilih untuk disimulasikan menggunakan ANSYS Fluent v16. Simulasi aerofoil dijalankan untuk memerhati tindakbalas aerofoil dalam aliran angin. Dua kategori simulasi dijalankan menggunakan Reynolds Number 10^5 & 10^4 . Sistem yang mempunyai kekakuan yang berbeza digunakan. Keputusan dari simulasi menunjukkan bahawa Nombor Strouhal kekal pada 0.732 walaupun perubahan dalam kekakuan system dan Nombor Reynolds.



ACKNOWLEDGEMENT

Firstly I would like to thank God for giving me this opportunity to study in UTeM and having this chance to complete my Final Year Project.

Dr. Cheng See Yuan who is my supervisor deserve my gratitude and appreciation. Thank him for giving me this opportunity to carry out my final year project research with him. His guidance throughout the whole year and encouragement when I needed it most has supported me both physically and mentally.

Secondly, I would like to thank my family members that gave me mental support until the completion of this project. My friends, coursemates who have been with me through thick and thins makes me who am I today. They too deserve my gratitude.

Last but not least, I want to thank UTeM for equipping me with knowledge, providing instruments for us to learn more efficiently and all the lecturers who have taught me since the time I stepped into UTeM. Without all of that, I wouldn't probably be able to complete my Final Year Project.



TABLE OF CONTENTS

	PAGE
DECLARATION	
DEDICATION	
ABSTRACT	i
ABSTRAK	ii
ACKNOWLEDGEMENT	iii
TABLE OF CONTENTS	iv
LIST OF FIGURES	vi
LIST OF TABLE	viii
CHAPTER	
1. INTRODUCTION	1
1.1 Background	1
1.2 Problem Statement	2
1.3 Objectives	3
1.4 Scopes Of Project	3
2. LITERATURE REVIEW	4
2.1 Fluid Structure Interaction (FSI)	4
2.1.1 Vortices Induced Vibration (VIV)	5
2.1.1.1 Factors Affecting VIV	6
2.1.1.2 Wake Region in VIV	7
2.2 Airfoil	8
2.3 Mass Spring Damper System	10
2.3.1 Natural Frequency	11
3. METHODOLOGY	12
3.1 Computer Aided Engineering (CAE)	15
3.2 Identification of Cross-Section	15
3.3 Geometry Drawing	15
3.4 Mesh Generation	16
3.5 Solver	18
3.6 Pre-Processing	19
3.7 Flow Chart	20
4. RESULT AND DISCUSSION	21
4.1 Fix Body Simulation	21

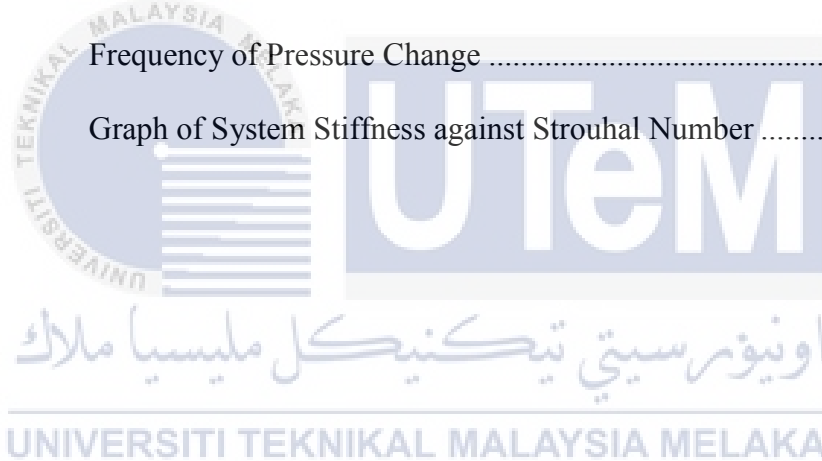
4.2	Grid Independence Test	23
4.3	Stiffness vs Body Motion	24
4.4	Stiffness vs Strouhal Number	30
4.5	Discussion on Non-Existence of Fluid Structure Interaction	36
5. CONCLUSION AND RECOMMENDATION		38
REFERENCES		40
APPENDIX A Gantt Chart PSM I		45
APPENDIX B Gantt Chart PSM II		46



LIST OF FIGURES

FIGURE	TITLE	PAGE
2.1	Detailed Sketch Of Flow Near Separation (Hansen et al., 2015)	6
2.2	Relationship of Airfoil Performance and Its Dimension (Ahzalilov, 1996)	8
2.3	Vortex Generation From End Plates (Meederira, 2014).....	9
2.4	Mass-Spring-Damper System	10
3.1	Mesh Setup for circle.....	13
3.2	User Defined Function using 6DOF	14
3.3	Mesh Generation for NACA0018 Airfoil.....	17
4.1	Flow Separation At Rear End Of NACA0018 Airfoil.....	21
4.2	Vortex Street Formation	22
4.3	Fluctuating Lift Force for a Fixed Airfoil System.....	23
4.4	Frequency of Lift Graph for Fixed Airfoil System.....	23
4.5	Lift Data Trend for Grid Independent Test (Lift Magnitude & Strouhal Number).....	24
4.6	UDF Setting for NACA0018 Airfoil – 1DOF Motion	25
4.7	Motion of Airfoil in Y-Axis with RE100,000 and Stiffness 50K.....	26
4.8	CG Motion of Airfoil System with Natural Frequency 1.59Hz	26
4.9	Frequency of CG Motion Natural Frequency 1.59Hz	27
4.10	CG Motion of Airfoil System of Natural Frequency 5.03Hz	27
4.11	Frequency of CG Motion Natural Frequency 5.03Hz	28

4.12	Graph of System Stiffness against Body Movement along Y-Axis	30
4.13	Lift Data NACA0018 with Natural Frequency 1.59Hz.....	30
4.14	Frequency of Lift Data NACA0018 with Natural Frequency 1.59Hz..	31
4.15	Lift Data NACA0018 with Natural Frequency 5.03Hz.....	31
4.16	Frequency of Lift Data NACA0018 with Natural Frequency 5.03Hz..	32
4.17	Lift Force Comparison for Different System Stiffness in Simulation Time	32
4.18	Monitor Point Setup To Collect Pressure Changes Due To Vortex Shedding	33
4.19	Pressure Fluctuation at Vortex Street	33
4.20	Frequency of Pressure Change	34
4.21	Graph of System Stiffness against Strouhal Number	35



LIST OF TABLE

TABLE	TITLE	PAGE
3.1	Validation Result	14
4.1	Grid Independent Test on Fix Airfoil Profile	24
4.2	System with Different Stiffness	25
4.3	Data Comparison for System Stiffness and Body Motion	29
4.4	Comparison System Stiffness with Strouhal Number	34
4.5	Comparison Between Vortex Shed Frequency & Airfoil Motion Frequency for $Re_{100,000}$	35
4.6	Overall Result Comparison	36

CHAPTER 1

INTRODUCTION

1.1 Background

An object subjected to flowing fluid will experience a phenomenon known as fluid structure interaction. This interaction will generate resultant force that is resolved into the lift and drag directions for convenient in the analysis.. When fluid encounter a blunt object, wake region will present behind the body where back flow takes place. One types of wake is in vortices form. This phenomenon is due to separation of boundary layer that bounds the wake and free stream which leads to fluid rotation. These rotating fluid result in formation of individual vortex which sheds at the rear end of the body and travel down the wake. Typically, an vortex shedding which is periodic and in alternating form will take place in the wake field, this is called a vortex street.

At some instances, the vortex shedding has a pattern which is not symmetrical about the body. There are some vortices being shed on the top surface of the body and some are at the bottom of the surface. This will cause irregular pressure distribution on the body hence causing lift force at both sides of the body to be exerted periodically. This occurrence is known as vortices induced vibration (VIV). This periodic shedding action has its own frequency. When the body's natural frequency matches with the frequency of this oscillation, „Lock-in“ or also known as resonance will happen. This will amplifies the body amplitude of vibration creating displacement on the object.

A fixed body experiencing fluid induced vibration will have a different wake region when compared to an elastically mounted body which is allowed to move. These elastically mounted bodies will experience a motion which is in translation or rotation or both. This means that the body will move whenever there is a fluid induced effect on the body. At this moment the wake region of the body might be affected as the moving body will cause a change in the body orientation. When the wake region changes it will affect lift and drag forces of the body in the flow field. Hence it is important to know whether the body motion affects flow behaviour when compared to a fixed body where the wake is constant throughout.

1.2 Problem Statement

There are numerous objects of various shapes that experience fluid flow for example house, bridge, fan, trees etc. Fluid structure interaction is the phenomena that occurs when a flowing fluid encounters an object. During this interaction, the objects will respond in a particular way due to the flowing fluid. This is known as the fluid induced effect. In many simulations, the response of a body which sometimes comes in translational and rotational manner or even deformed object is neglected. This reduces the simulation time and simplifies the simulation case. However in real life situation, this response of the body is present and might cause changes to the properties or performance of the system.

Different cross-sectional objects will react differently. In this project an airfoil cross-section shape is chosen to be investigated. This is because there are lots of airfoil applications around us for example the spoiler of a car, the wing of an airplane, blade of a helicopter, blade of a fan, blade of a wind turbine and blade of a compressor rotor.

The vortex induced vibration on the airfoil will be investigated in this project. A fixed airfoil and an elastically mounted airfoil will be set up. Changes in vortex shedding

frequency, magnitude of lift force and magnitude of airfoil movement along the y-axis will be determined by manipulating the stiffness of the system and the fluid's Reynolds Number.

1.3 Objectives

The objectives of this project are as follows:

- To identify flow behaviour in fixed body simulation and moving (1DOF) rigid body simulation
- To examine impact of body motion on flow characteristics
- To identify the vortex shedding in wake region of airfoil.
- To observe the effect of aerodynamic forces on an elastically mounted airfoil

1.4 Scopes Of Project

The scopes of this project are:

- Fixed airfoil simulation to identify vortex shedding
- Simulation of elastically mounted (1DOF) airfoil (rigid body) with different stiffness
- Compare the changes in airfoil response in fixed and elastically mounted simulation

CHAPTER 2

LITERATURE REVIEW

2.1 Fluid Structure Interaction (FSI)

Fluid Structure Interaction is the phenomenon that occurs at the interphase between an object and the surrounding environment fluid. Whenever fluid flow passes a stationary object or a moving object moving pass a stationary fluid domain, there will be effect imposed by both the fluid and object on each other. Happenings of FSI which can be seen at for instance oil-rig risers and bridge (Zahari & Dol, 2014) and in medical tools (Hessenthaler et al., 2016) involve the coupling of unsteady fluid flow and structure motion. The mechanism that causes elastic structure to vibrates and turn to self-excite while submerge in a flowing fluid is hard to estimate and predict due to mechanical properties of structures and properties of the fluid itself.

There are experiments carried out to investigate flowing fluid relationship with the structure it is impose on, result shows that they are both highly interrelated elements. In Chee Chew Wong articles, (2011) metal plates in laminar flow is studied and the transient response of the plates under FSI conditioned is determined. Validation for FSI cases through real time investigation and experiments is vital to prove the simulations obtained from Computer Aided Engineering Tools are trustworthy. Lienhart & Pereira Gomes, (2006) uses Particle Image Velocimetry to measure flow field and structure deflection in validating their results. A two dimensional reference structure of a cylinder is immersed in laminar and turbulent flow to examine their interaction behaviour. Therefore simple structure such as cylinder or plate to complex structure such as bridge (Hansen et al., 2015)

which experience FSI are among the topic of interest of structural engineers as they provides useful and reliable information to the objects in our daily lives.

2.1.1 Vortices Induced Vibration (VIV)

Vortices Induced Vibration (VIV) is a typed of FSI that happens on a structure. This is an effect of vortices shedding in the wake flowing through bluff body structure such as column, risers and mooring lines. Structure Hydrodynamic loading will be affected by change in vortices which will cause structure to vibrate (Nguyen & Nguyen, 2016). VIV occurs when pressure on surface fluctuates; this leads to fluctuates of lift force thus producing cross stream oscillation. These oscillations sometimes can be large and sometimes is too small to notice depends on the wake behind the object. Gharib, (1999) experiments using cylinder of various mass ratio states that the vortex wake tends to be almost identical regardless of the geometry being simulated. This also means that object subjected to fluid flow will experience either little or a large amount of vortex wake where fluid separation occur at the rear end of the body. There is presence of vortex shedding behind the race car clean wing and a shear layer between regions of positive and negative vorticity (Kuya, et al, 2009). This confirms that although the wind is aerodynamic in size, there is also vortex formation which is due to wake region.

Hansen, (2007) carried out an experiment in wind tunnel using geometry with different cross-section. Among the tested geometries are circular cylinder, sharp-edged sections, octagons and bridge decks. From the result of Hansen, (2007), significant vibration level will causes displacement of structure when the wind reaches slightly above 6m/s. This shows activity of VIV on these structures with different cross-section caused by the flowing wind.

Besides of VIV which is directly related to the FSI, there is also Wake Induced Vibration (WIV) which also has a similar effect when compared to VIV. The difference is

that WIV happened only when there is wake region that contains sufficiently large pressure differences or also can be known as Karman Vortex Street.

2.1.1.1 Factors Affecting VIV

In Pantazopoulos & Pantazopoulos findings, (1994), they state that important parameters in VIV are lift coefficient, shedding frequency (Strouhal number), correlation length and shedding frequency bandwidth. Hansen et al., (2015) mention VIV measured in dynamic test rig depends strongly on Reynolds Number. Bluff bodies surface will always experience region of vorticity where flow is more or less coherent. Figure 2.1 (Hansen et al., 2015) provides clear visualization on the flow separation region on bluff body where back flow occur which leads to formation of small vortices in the shear layer region near the boundary of the object. On sharp-edge body separation flow defined by location of edges while rounded bodies depends on air velocity which is also directly related to Reynolds number.

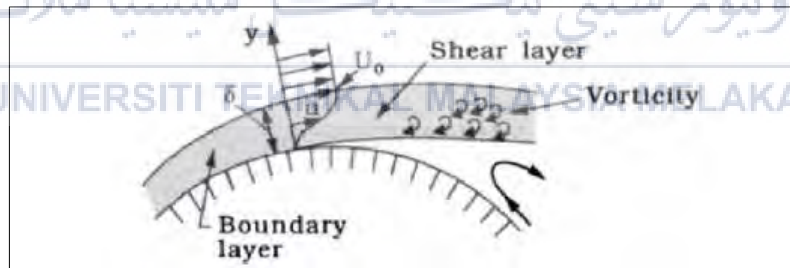


Figure 2.1: Detailed Sketch Of Flow Near Separation (Hansen et al., 2015)

Hansen et al., (2015) uses different configuration of streamlined single box grinder to investigate the effect of VIV. It is found that Strouhal number increase with Reynolds number and the resonance wind velocity for VIV is governed by Strouhal number.

During vortex formation, when the vortices are not produced symmetrically with respect to the mid-plane of the body, different lift forces formed at each side of the body leading to

motion tranverse to the flow. Strouhal Number which is an important term in vortex shedding is shown in equation below.

$$S = \frac{f_v D_c}{V} \quad (2.1)$$

Where f_v is the vortex shedding frequency at rest, D_c is the diameter of circular cylinder and V is the velocity of ambient flow. Frequency of vortex shedding is related to Reynolds number, Re which is also linked to flow velocity, viscosity of fluid and characteristic length of object (Abhiroop Jayanthi, 2008).

A new parameter termed „effective stiffness“ by Gharib, (1999) will also affect the chances of VIV. By reducing the structure to fluid mass ratio, lock-in behaviour or resonance can also be prevented. However it is also found out that at low mass ratio, VIV can occur with or without lock-in behaviour. Self-excite oscillation and forced oscillations are the types of VIV where self-excited oscillation occurs naturally and forced oscillation can be controlled independently of fluid velocity.

2.1.1.2 Wake Region in VIV

Williamson & Govardhan, (2004) uses an elastically mounted cylinder as an example for VIV system. Certain wake pattern is induced by body motion for example the 2P, 2S, P, C and S mode. These are all due to imbalance pressure distribution across the surface of the body of cylinder when fluid flows pass it.

An object experiencing fluid flow will experience two effects which is drag force and lift force. When an object subjects to VIV, fluctuating lift force can be seen on a body. When the pressure of both upper and lower side of the object fluctuates with time, the lift will be affected too. These are dimensionless coefficients defined by:

$$C_L = \frac{F_L}{\frac{1}{2}\rho V^2 A_L} \quad (2.2)$$

$$C_D = \frac{F_D}{\frac{1}{2}\rho V^2 A_D} \quad (2.3)$$

Where F_L and F_D are the lift and drag forces, ρ is the density of the fluid and V is the velocity. A_L and A_D are reference area. The size of the wake region will determine the magnitude of these two forces acting on the body(Lienhard, 1966).

2.2 Airfoil

Airfoil shape is used in car spoiler and wing, this shape is usually inverted to provide desired effects. Inverted airfoil has a low pressure suction region on the lower surface and high pressure suction region on the higher surface of airfoil geometry. Airfoil geometry can be summarize by few parameters for example are maximum thickness, maximum chamber, position of max thickness and many more. Ahzalilov, (1996) found out that shape of pressure distribution relates closely to airfoil performance as shown in Figure 2.2. It is shown that the geometry or design of the cross-section will cause the pressure distribution across the airfoil surface to change. Holmes, (2008) state that large wing surface area creates more lift while the increase of aspect ratio will induce less air resistance. Breu,et al, (2008) also mention that the drag reduction of a vehicle by implementing a rear spoiler is strongly dependent on the shape of spoiler.

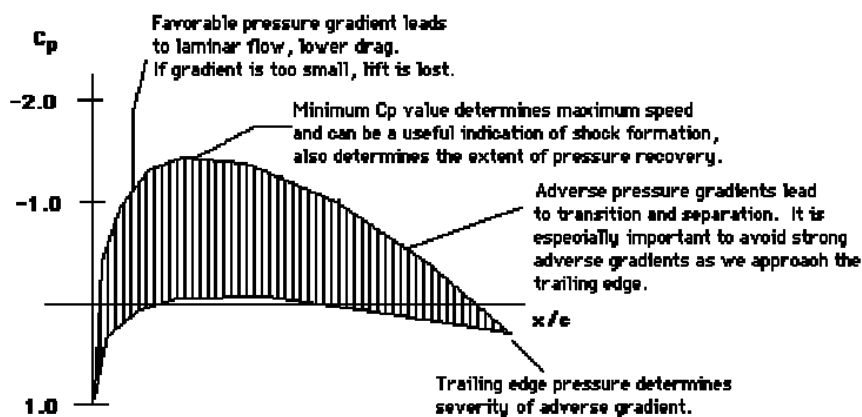


Figure 2.2: Relationship of Airfoil Performance and Its Dimension (Ahzalilov, 1996)

Since most aerofoil profile is used in airplane to create a large lift while taking off, by inverting the shape it will create a sufficient negative lift force also known as down force on the vehicle. Stiffness of system will affect the behaviour of the aerofoil which the dynamic response of the aerofoil is dependent on the location of pitching axis says (Z.Peng, 2009). Experiment on spoiler effect on wake region was carried out by et al, (2011) and its found out that the deflection of spoiler enlarge the wake region by 0.79%. Tsai, et al, (2009) also found out that by installing spoiler, lift coefficient can be reduced which leads to improved high speed driving condition and vertical stability of driving. From the experiment, when spoiler is placed on the trunk top, drag coefficient increase while lift coefficient decreases. Trailing vortex that is similar to that of a flying plane is produce due to pressure difference on the upper and lower surface of spoiler. This phenomenon also occurs in the work of Meederira, (2014) which saw vortex generation from end plates which can be seen in Figure 2.3. This shows that fluid flowing pass a airfoil profile will generate vortex in the wake region.

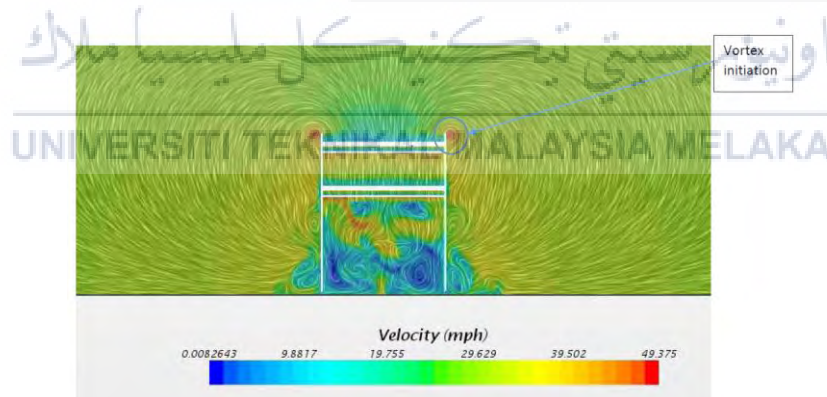


Figure 2.3 Vortex Generation From End Plates (Meederira, 2014)

Meederira, (2014) result indicates that when the AOA is increased, separation region behind the body become more obvious. This separation flow will affect the lift and drag force induced on the body. Kieffer, et al, (2006) and Meederira, (2014) found out that hydrodynamic performance of foils will be affected by the Angle of Attack (AOA) of the foils. Holmes, (2008) state the coefficient of lift increases with increasing angle of attack

however at some angle flow separation happens and enlarge which will reduce the lift coefficient. Huang (2011) states airfoil when placed at post-stall angle of attack might response as if a bluff body. Flow separation problem can be tackle through element of high aspect ratio. Other than that, endplates of the rear wing in 3D simulation avoid trailing vortices formation which is due to air leakage in wing tip. Experiments carried out by Elsayed et al., (2011) found out the fixing spoiler on aircraft wings is able to accelerate vortex breakdown in the wake region. By deflection spoiler by 10° peak vorticity value is reduced to 0.46.

2.3 Mass Spring Damper System

Mass spring damper system is used in many experiments especially those that involve object's motion. Equation that govern the object in this system is $m\ddot{x} + b\dot{x} + kx = W$ shown in Figure 2.4. Zhang & Ji, (2016) uses an elastically mounted 2DOF system that include an airfoil and circular shape.

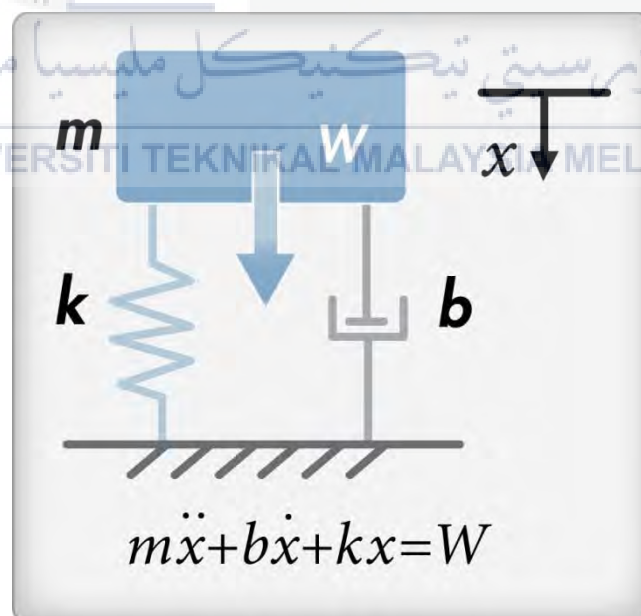


Figure 2.4 Mass-Spring-Damper System

Motion of object is differentiate into 6 types, translation in x, y & z axis and rotational motion in x, y & z axis.

2.3.1 Natural Frequency

The natural frequency of a system is the frequency where system oscillates when it is acted by an external force. The natural frequency of a system is calculated by,

$$F_N = \frac{1}{2\pi} \sqrt{\frac{k}{m}} \quad (2.4)$$

Resonance or lock-in occurs when the natural frequency of the structure is in sync with the frequency of an outside force. During this period, exceptionally strong response will be obtained from the structure causing the structure to vibrate or moves with great amplitude. In Derakhshandeh, et al, (2016) free-decay tests are conducted to obtain the natural frequency of the fundamental bending mode of the cantilevered aerofoil. From the dynamic response of the subject, 4.70Hz is the natural frequency of the cantilevered beam which is away from the frequency of oscillation hence structure does not experience resonance effect.

For the unsteady pressure at the wake vortices to induce the body to response, Williamson & Govardhan, (2004) found out that the vortex formation frequency has to be closed enough to the body natural frequency. Besides from this finding, it is also found out that bodies can conceivably vibrates at high amplitude at hundreds of times the natural frequency. Sufficient large body movement during this phenomena may affect the wake flow according to Gharib, (1999). The vortex growth period and phase can be affected resulting in stronger vortices with altered patterns. This will cause an increase in spanwise correlation of the wake, drag and lift. Results found that 40% of vortex shedding frequency can be shifted and this effect are not only limited to circular cylinders.

CHAPTER 3

METHODOLOGY

Circle shape is the most common cross-section used in Vortex Induced Vibration study such as by Singh & Mittal, (2005) and Maysa, et al, (2016). The shape or cross-section of the object to be studied needed to be determined. Review from previous study found out that there are lots of researches on airfoil profile in laminar flow but there are not many studies on turbulent flow. Hence this work will focus on turbulent flow across airfoil cross-section shape. The shape of airfoil comes in many while most profiles are based on NACA number. A symmetry profile of NACA0018 which has been investigate its properties by Nakano, et al, (2007) is chosen to be investigated.

First and foremost the formation of vortex is to be observed behind the airfoil. This is done to show vortex shedding behind airfoil profile as found by Meederira, (2014). If vortex shedding is not observed, the angle of attack, AOA of the airfoil is adjusted and re-run the simulation. After obtaining steady vortex shedding, fast fourier transform, FFT is done on the oscillating lift data to find its peak frequency which is the vortex shedding frequency.

The next part of this project will be carried out by allowing translation motion of the rigid airfoil body. A user defined function, UDF which uses 6 degree of freedom, 6DOF is applied to the rigid body. The feasibility of this UDF is validated by running a simulation using a circle as our object which is carried out by Singh & Mittal, (2005). Simulation with a non-dimensional mass of 10, reduced velocity of 4.6 and Reynolds Number of 100 is carried out by allowing transverse and in-line motion of circle.

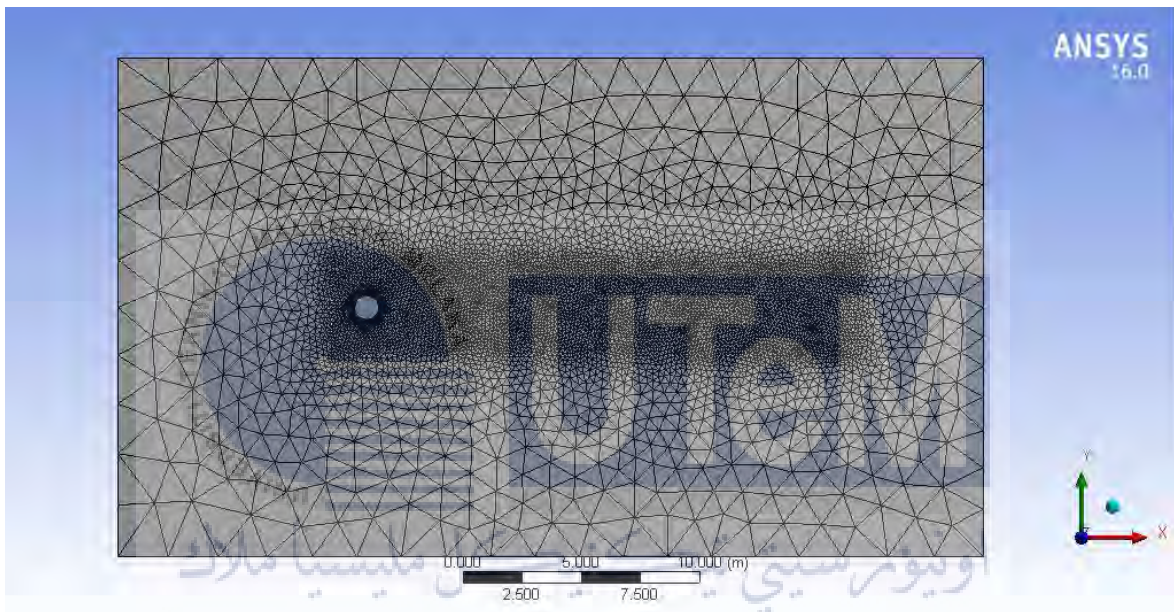
$$U^* = \frac{U_\infty}{f_n D}; \quad (3.1)$$

$$m^* = \frac{4m}{\pi p_\infty D^2}; \quad (3.2)$$

$$\text{Reynolds Number, } Re = \frac{\rho_\infty U_\infty D}{\mu_\infty}; \quad (3.3)$$

U^* : Reduced Velocity; U_∞ : Free Stream Speed; D : Characteristic Length;

m^* : Non-Dimensionalize Mass; m : Mass; p_∞ : Density.



UNIVERSITI MELAKA Figure 3.1: Mesh Setup for circle

Finer mesh is generated around the circle and the region behind the cylinder as shown in Figure 3.1 to capture the boundary layer around the circle and the wake region behind the circle. Viscous Model with laminar flow, transient time simulation, Dynamic Mesh with UDF of 6DOF shown in Figure 3.2, Simple Scheme with Second Order Transient Formulation and time step of 0.0625s are the setting used for this simulation.

```

#include "udf.h"
#include "dynamesh_tools.h"
#include "unsteady.h"
DEFINE_SDOF_PROPERTIES(cylinder, prop, dt, time, dtime)
{
double F_disturbance_X;
double F_disturbance_Y;
double M_disturbance_Z;
double K_X;
double K_Y;
double Damping_X;
double Damping_Y;
double CG_X;
double CG_Y;
prop[SDOF_ZERO_TRANS_X] = FALSE;
prop[SDOF_ZERO_TRANS_Y] = FALSE;
prop[SDOF_ZERO_TRANS_Z] = TRUE;
prop[SDOF_ZERO_ROT_X] = TRUE;
prop[SDOF_ZERO_ROT_Y] = TRUE;
prop[SDOF_ZERO_ROT_Z] = TRUE;
prop[SDOF_MASS] = 2.5;
prop[SDOF_IZZ] = 1;
K_X = 466.43;
K_Y = 466.43;
Damping_X = 0;
Damping_Y = 0;
CG_X = 0;
CG_Y = 0;

if(time <= 0){
F_disturbance_X = 0;
F_disturbance_Y = 0;
M_disturbance_Z = 0;
} else {
F_disturbance_X = 0;
F_disturbance_Y = 0;
M_disturbance_Z = 0;
}
prop[SDOF_LOAD_F_X] = F_disturbance_X - K_X*(DT_CG
(dt)[0]-CG_X) - Damping_X*DT_VEL_CG(dt)[0];
prop[SDOF_LOAD_F_Y] = F_disturbance_Y - K_Y*(DT_CG
(dt)[1]-CG_Y) - Damping_Y*DT_VEL_CG(dt)[1];
prop[SDOF_LOAD_M_Z] = M_disturbance_Z;
}

```

Figure 3.2 User Defined Function using 6DOF

By implementing the UDF into simulation, result of mean drag coefficient and Strouhal number of circle due to vortex shedding frequency is shown in Table 3.1. Value of mean drag coefficient obtain is identical with the value found by Singh & Mittal, (2005) while the Strouhal number obtained differs by 12.27%. Hence the simulation settings and function of this UDF is validated.

Table 3.1 Validation Result

	Mean Drag Coefficient, Cd		Strouhal Number, St	
	Magnitude	Percentage Difference		Percentage Difference
S.P. Singh, S. Mittal (2005)	1.31	0%	0.163	12.27%
Experiment Result	1.31		0.143	

The UDF with 6DOF is then applied to the airfoil which allows transverse motion for the airfoil. Data for lift coefficient and centre of gravity of airfoil are extracted from simulation to be analysed.

3.1 Computer Aided Engineering (CAE)

This project is carried out using Computer Aided Engineering (CAE) software. Computational Fluid Dynamics (CFD) and Finite Element Analysis (FEA) are used. CFD is a branch of fluid mechanics that uses algorithm and numerical method to solve and analyse fluid flows problems. One of the advantages is the cost to construct actual prototype can be saved.

3.2 Identification of Cross-Section

Airfoil shape is chosen due to its vast usage in engineering field for example the blades inside a turbine, wing of race car, blades of fan, the wing of an airplane and blade of a helicopter. There are researches using airfoil profile to study the wake region behind the geometry. Most of them are carried out in laminar flow while there are little studies carried out in turbulent flow. For instance, NACA 9514 (Meederira, 2014), NACA0012 (Derakhshandeh et al., 2016)&(Shan, Jiang, & Liu, 2005), and NACA4412 (Vinuesa, Hosseini, Hanifi, Henningson, & Schlatter, 2016). All of these airfoil shapes are simulated to obtain the lift and drag force induced on the geometry while fluid flowing passes it. In this study, NACA0018 which is a symmetry airfoil profile is selected. Properties of NACA0018 can be found at (Airfoil Tools).

3.3 Geometry Drawing

The coordinates needed to draw NACA 0018 profile is obtained from (Airfoil Tools). The coordinates are set to .txt file then imported into Geometry-Design Modular. The points are connected using „Line“ and the trailing edge of profile is adjusted using

„VertexBlend“ which gives a round edge at the trailing edge. The domain is created with 2 chord length in-front of the profile, 9 chord lengths behind the profile and 1.5 chord length above and below the profile. A smaller domain is created closed to the profile for body of influence purposes.

In order to observe the wake region clearly, there are a lot of studies which tilt the airfoil profile which performing numerical simulation. In a study (Mertins, Elsholz, Barakat, & Colak, 2005) , the strength of vortices formed by aileron side faces is minor when compared to the tip vortex. However the outboard spoiler at 30 degree deflection produces a significant stronger vortex. Vinuesa et al., (2016) carried out a direct numerical simulation on NACA4412 with $Re=400,000$ and $AOA=5^\circ$. They observed instantaneous vertical structural formation on upper & lower side when flow is tripped at 10% chord length. NACA0025 airfoil, chord length of 0.3m was investigated by Yarusevych, Sullivan, & Kawall, (2009). Range of Re and AOA is 55,000 to 210,000 and $0^\circ, 5^\circ, 10^\circ$ respectively. In another experiment using turbine blade NREL S809 by Pellegrino & Meskell, (2013) vortex shedding found out to be in the range of $0.11 < St < 0.16$. Simulation properties are RANS SST model at $Re=1,000,000$ and high angle of attack. Range of AOA is $\alpha = [40^\circ \text{ to } 140^\circ]$, $\alpha = [-40^\circ \text{ to } -150^\circ]$. Hence in order to visualise vortex shedding in the flow, the horizontal profile of NACA0018 is rotated to 16 degree which is approximate the stalling angle for airfoil profile.

3.4 Mesh Generation

There are a lot of experiments being done on vehicle using CFD with various different methods and meshing. In Hetawal, et al., (2014) and Breu et al., (2008) , triangular meshing is used for its proximity for changing curves and bends to attain unstructured grid. Triangular elements adjust easily to complex body shapes. For the meshing done on structure before simulation, the region around race car model are intended to be much

denser to capture the near boundary flow(Wang, et al, 2010). Likewise for Olsson, (2014) prism cell inflation layer was created near car body. Program controlled inflation layer is used in Hetawal et al., (2014) to get the boundary layer effect and transition SST 4 equation model is chosen. In Meederira, (2014) similar actions are done on the wing assembly to closely monitor the flow separation. Besides that, region behind the body was added mesh refinement due to expected turbulent flow. Finer mesh maintains the curvature of body hence able to simulate object which are almost identical in real life geometry.

For the mesh of NACA0018, all triangles method is used. Inflation of first layer thickness with height of 0.1mm, 35layers and growth rate of 1.1 is done on the surface of the airfoil to capture the boundary layer of the object. Finer cell of 35mm is created around the region of the profile using body of influence to ensure the simulation around the profile is done with higher precision. Edge sizing is done on the surface of airfoil. Smaller edge of 5mm is generated at curved region and slightly larger edge of 10mm on straight surface. Mesh is shown at Figure 3.3. The name selections are inlet, outlet, airfoil and sides.

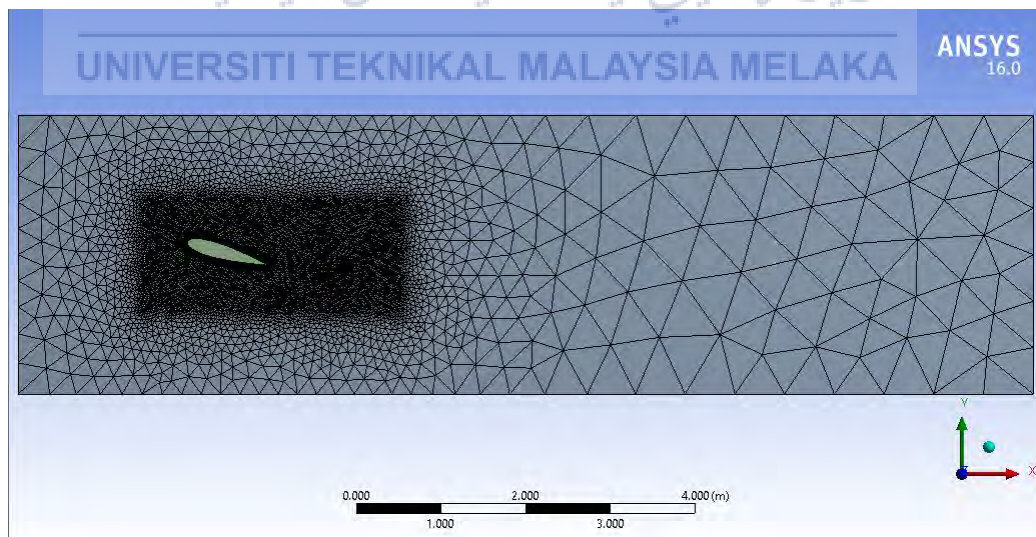


Figure 3.3 Mesh Generation for NACA0018 Airfoil

3.5 Solver

The setup before simulation is important to be able to produce trustworthy result. Numerical simulation is conducted by Tsai et al., (2009) to analyse pressure field, velocity vector field and aerodynamic noise of a car. Stability of forces induced by fluid flow around the car was also identified using RNG $k-\Omega$ turbulence model. K- ϵ turbulent model stands out better than LES in this case to predict the flow field across the vehicle surface. Result from simulation of transient flow in high Reynolds Number can sometime be unpredictable due to its unsteady properties. In Nguyen & Nguyen, (2016) DES approach for VIV simulation for high Reynolds Number is investigate. Hybrid approach based on URANS model, $k-\Omega$ SST simplifies the procedure greatly. A hybrid RANS/LES model was chosen for simulation over cylinders in this study.

Transient simulations were carried out using the unsteady solver for the incompressible flow of Newtonian fluids on a moving mesh using the PIMPLE algorithm combining SIMPLE (Semi-Implicit Method for Pressure-Linked Equations) for sub-step convergence and PISO (Pressure implicit with splitting of operator) pressure velocity coupling. DES shows good accuracy in capturing unsteady vortex shedding phenomena with excellent prediction of the pressure distribution especially lift fluctuation. Mertins et al., (2005) used standard Wilcox $k-\Omega$ turbulence model in the experiment of spoiler and ailerons, while Meederira, (2014) uses Spalart-Allmaras model to simulate the wing assembly. Spalart-Allmaras is a one equation model for turbulent viscosity, it solves the whole flow region while not using any wall functions hence causing it less memory-intensive, quiet stable and shows good convergence. In CFD Fluent, for a more stable solution between each couple iteration, according to Olsson, (2014) the solution is started with first order accuracy, after it has converged, the solution is switched to second order accuracy.

For Setup process, transient analysis is done using SST k- Ω model. Reynolds Number is set to 10^5 . PISO Scheme is used with Bounded Second Order Implicit Transient Formulation. Drag and lift monitors are setup.

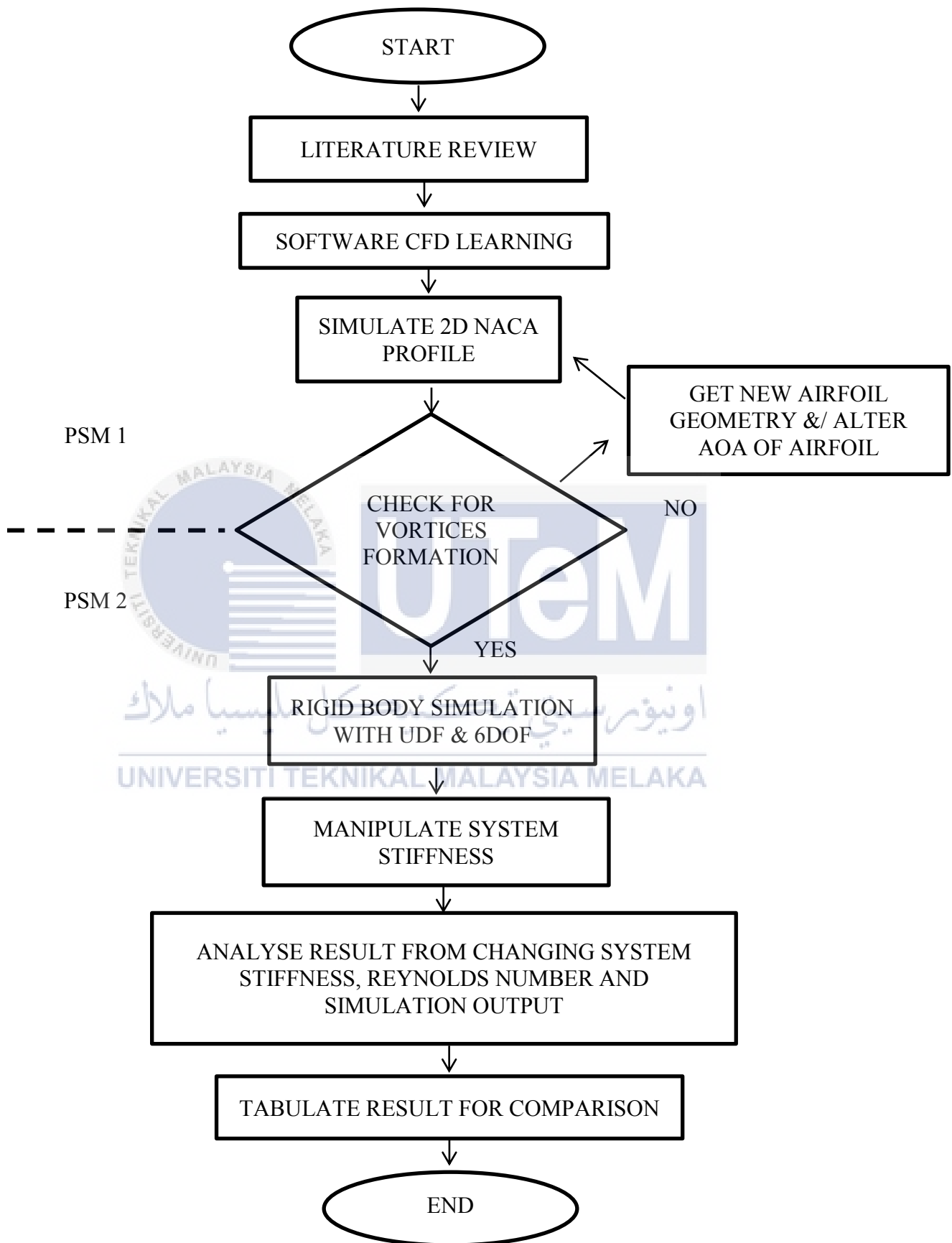
3.6 Pre-Processing

Hybrid Initialization is done and time step is set at $1e-05$ with 20 iterations per time step. Convergence criteria are set as state in the Table 3.2. Lift and Drag graph is obtained and observed. The contour plot for velocity, pressure and Q-Criterion is observed.

Table 3.2: Convergence Criteria

Residual	Convergence Criteria
Continuity	0.001
X-Velocity	0.001
Y-Velocity	0.001
K	0.001
Omega	0.001

3.7 Flow Chart



CHAPTER 4

RESULT AND DISCUSSION

4.1 Fix Body Simulation

From the fixed body simulation of the NACA0018 airfoil, flow separation occurs behind the object and there is significant backflow as shown in Figure 4.1. The setting of spoiler's AOA is at 16° which is about the stall angle for airfoil. Vortex shedding can be seen at Figure 4.2 and formation of vortex street is observed at the wake region.

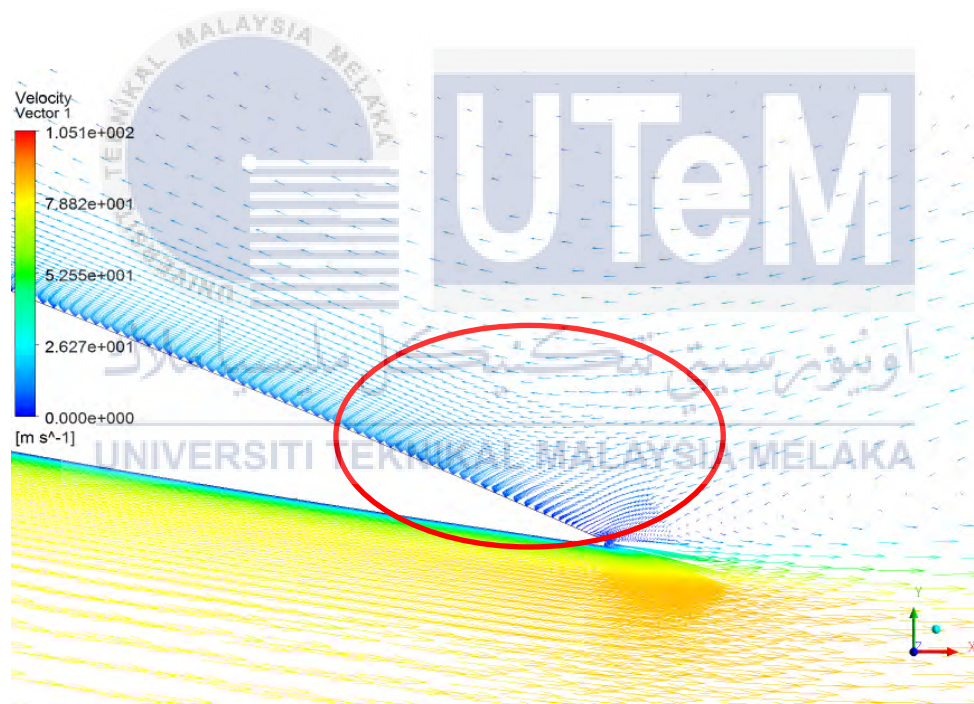


Figure 4.1: Flow Separation At Rear End Of NACA0018 Airfoil

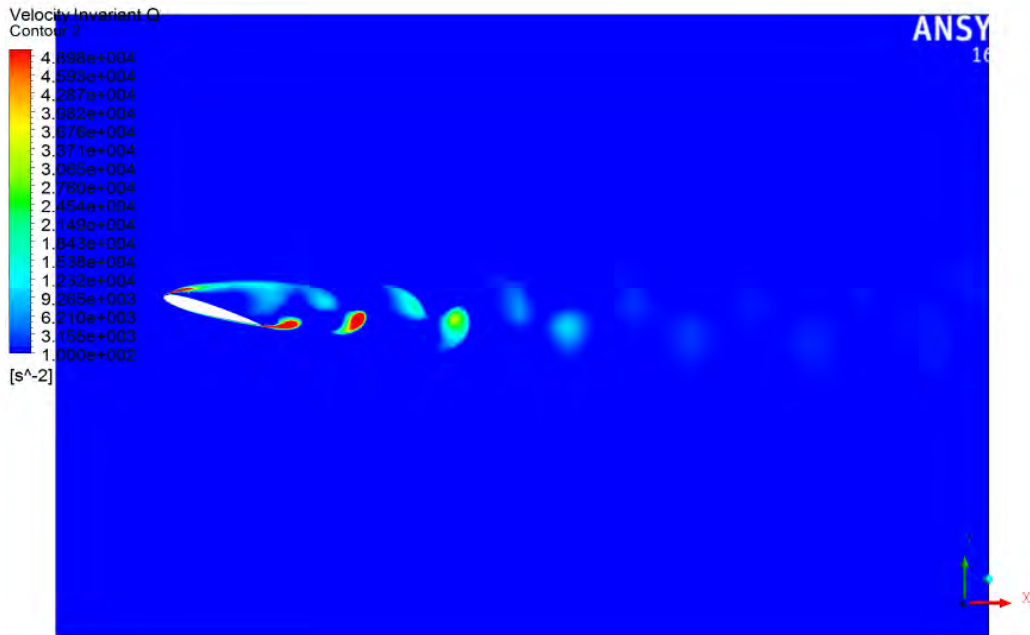


Figure 4.2: Vortex Street Formation

Samples data of lift force are obtain from post result and the lift graph is plotted as shown in Figure 4.3. It is observed that the lift force is fluctuating between a magnitude of 0.72 & 0.59. This indicates the pressure distribution on the upper and lower surface of the airfoil is changing periodically. This is due to vortex being shed in periodic manner as air flow passes the airfoil. When the FFT is done on the lift data, a frequency graph is plotted shown in Figure 4.4, it is observed that there is one significant peak on the graph which indicated the vortex shedding frequency of the airfoil which is at 73.2 Hz. Strouhal number, St of this frequency is 0.732.

$$St = \frac{F_v L}{U_\infty} = \frac{73.2 * 1}{100} = 0.732$$

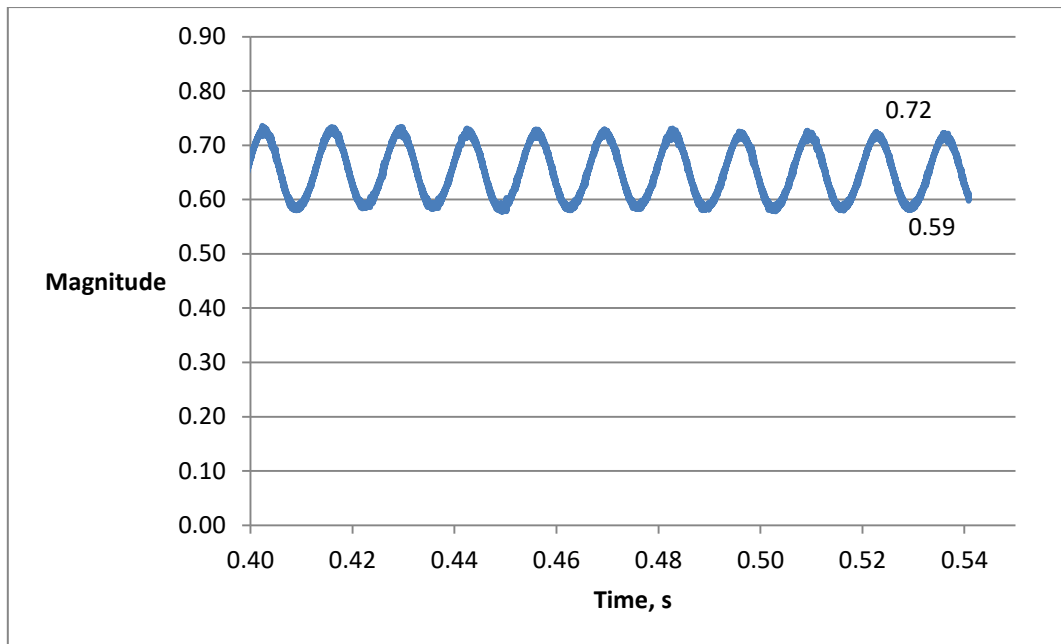


Figure 4.3: Fluctuating Lift Force for a Fixed Airfoil System

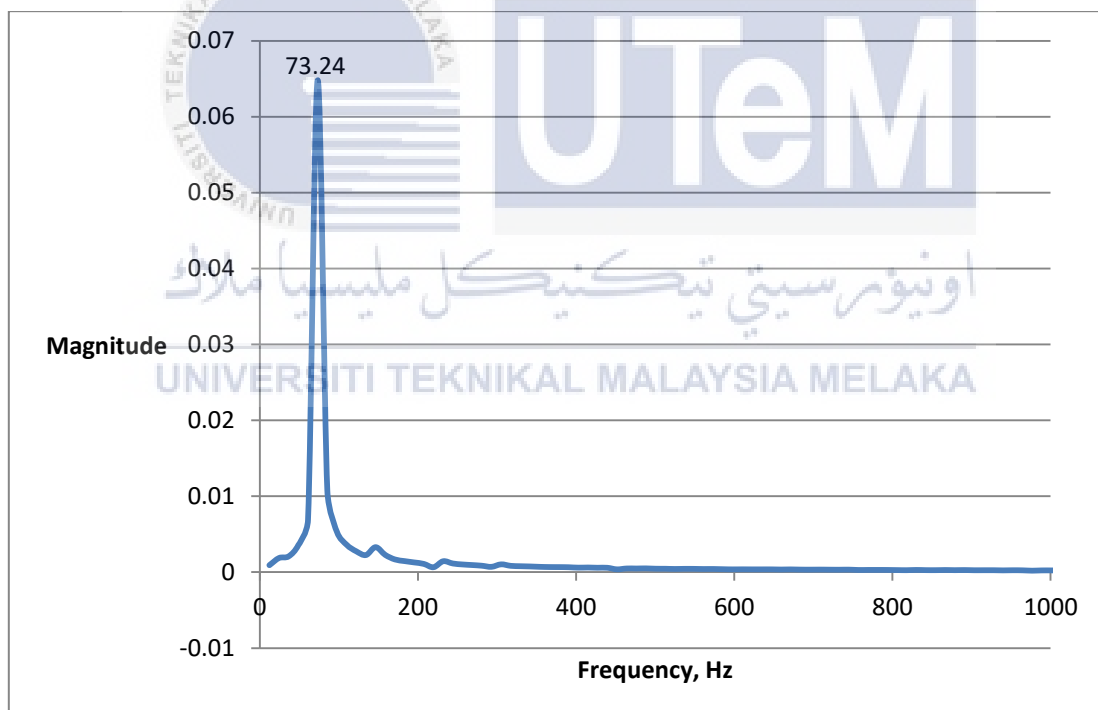


Figure 4.4: Frequency of Lift Graph for Fixed Airfoil System

4.2 Grid Independence Test

Grid independent test is done on this simulation to verify the accuracy of result obtained. Result shown in Table 4.1 proves the accuracy of result obtained from simulation. The strouhal number value for all 3 cases are identical while for the lift magnitude the range

of periodic fluctuation reduces. The fluctuation ranges is able to be measured more accurately due to finer mesh at the surrounding layer around the airfoil. This indicates that the data obtained is acceptable. The trend of lift data for all 3 test cases can be observe at Figure 4.5.

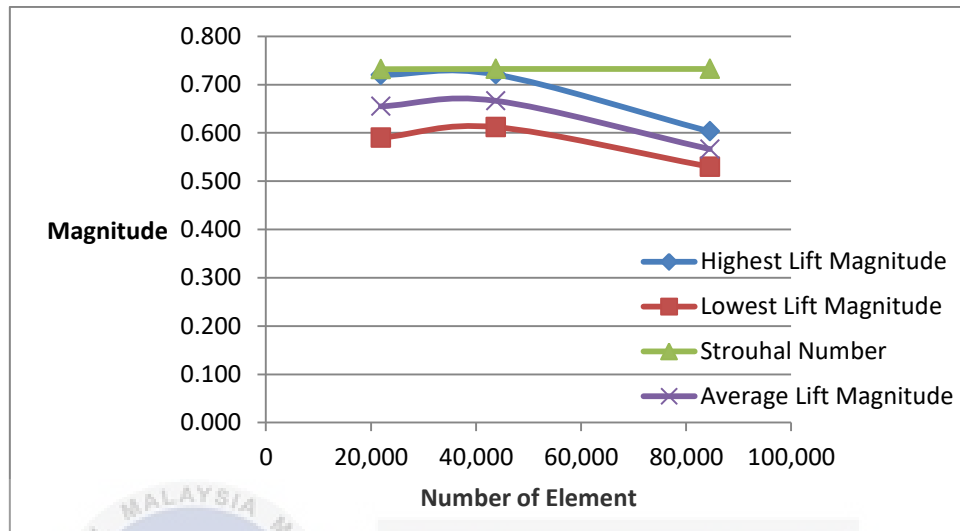


Figure 4.5 Lift Data Trend for Grid Independent Test (Lift Magnitude & Strouhal Number)

Table 4.1 Grid Independent Test on Fix Airfoil Profile

Number Of Element	Highest Lift Magnitude	Lowest Lift Magnitude	Average Lift Magnitude	Vortex Shedding Frequency	Strouhal Number
21,889(coarse)	0.720	0.590	0.655	73.200	0.732
43,735(media)	0.721	0.612	0.667	73.240	0.732
84,499(fine)	0.603	0.530	0.567	73.240	0.732

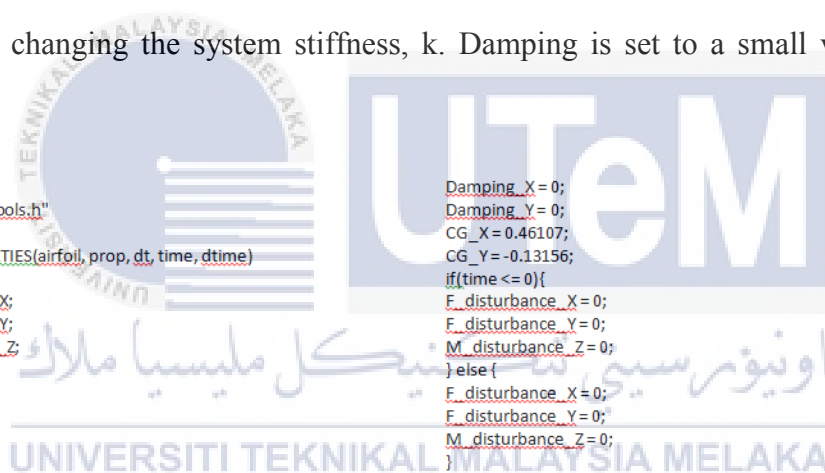
4.3 Stiffness vs Body Motion

Elastically mounted rigid body simulation is then done on the airfoil by allowing motion on y-axis. The airfoil is mounted by a mass-spring-damper system. Mass of airfoil, m given is 500kg which represent about the wing of an airplane. Several systems is deduced shown in Table 4.2 to have natural frequency approaching, match and higher than the vortex shedding frequency. This is to create a pre lock-in, lock-in and post lock-in cases where resonance occurs when natural frequency of system matches the vortex shedding frequency. Any changes in the output of lift force and system movement will be recorded.

Table 4.2 System with Different Stiffness

Stiffness	Natural Frequency	Reduced Frequency: f^*L/U
Fix	N/A	N/A
50,000	1.59	0.02
500,000	5.03	0.05
49,000,000	49.80	0.50
1,057,674,182	73.20	0.73
50,000,000,000	1591.50	1.59

Simulation is set at Reynolds Number of 100,000 and 10,000 which is turbulent flow with air as working fluid. The UDF of system is shown in Figure 4.6. Others system uses the same UDF by changing the system stiffness, k. Damping is set to a small value which is 0.001.



```

#include "udf.h"
#include "dynamesh_tools.h"
#include "unsteady.h"
DEFINE_SDOF_PROPERTIES(airfoil, prop, dt, time, dtime)
{
    double F_disturbance_X;
    double F_disturbance_Y;
    double M_disturbance_Z;
    double K_X;
    double K_Y;
    double Damping_X;
    double Damping_Y;
    double CG_X;
    double CG_Y;
    prop[SDOF_ZERO_TRANS_X] = TRUE;
    prop[SDOF_ZERO_TRANS_Y] = FALSE;
    prop[SDOF_ZERO_TRANS_Z] = TRUE;
    prop[SDOF_ZERO_ROT_X] = TRUE;
    prop[SDOF_ZERO_ROT_Y] = TRUE;
    prop[SDOF_ZERO_ROT_Z] = TRUE;
    prop[SDOF_MASS] = 500;
    prop[SDOF_IZZ] = 0.001;
    K_X = 50000;
    K_Y = 50000;
    Damping_X = 0;
    Damping_Y = 0;
    CG_X = 0.46107;
    CG_Y = -0.13156;
    if(time <= 0){
        F_disturbance_X = 0;
        F_disturbance_Y = 0;
        M_disturbance_Z = 0;
    } else {
        F_disturbance_X = 0;
        F_disturbance_Y = 0;
        M_disturbance_Z = 0;
        prop[SDOF_LOAD_F_X] = F_disturbance_X - K_X*(DT_CG(dt)[0]-CG_X) -
        Damping_X*DT_VEL_CG(dt)[0];
        prop[SDOF_LOAD_F_Y] = F_disturbance_Y - K_Y*(DT_CG(dt)[1]-CG_Y) -
        Damping_Y*DT_VEL_CG(dt)[1];
        prop[SDOF_LOAD_M_Z] = M_disturbance_Z;
    }
}

```

Figure 4.6 UDF Setting for NACA0018 Airfoil – 1DOF Motion

The movement of airfoil is observed from the changes in centre of gravity. For a stiffness of 50,000 N/m, the magnitude of airfoil movement along the y-axis is 160mm as shown in Figure 4.7 with a frequency of 1.52Hz. Both the data for lift in time domain and frequency domain is shown in Figure 4.8 and Figure 4.9.

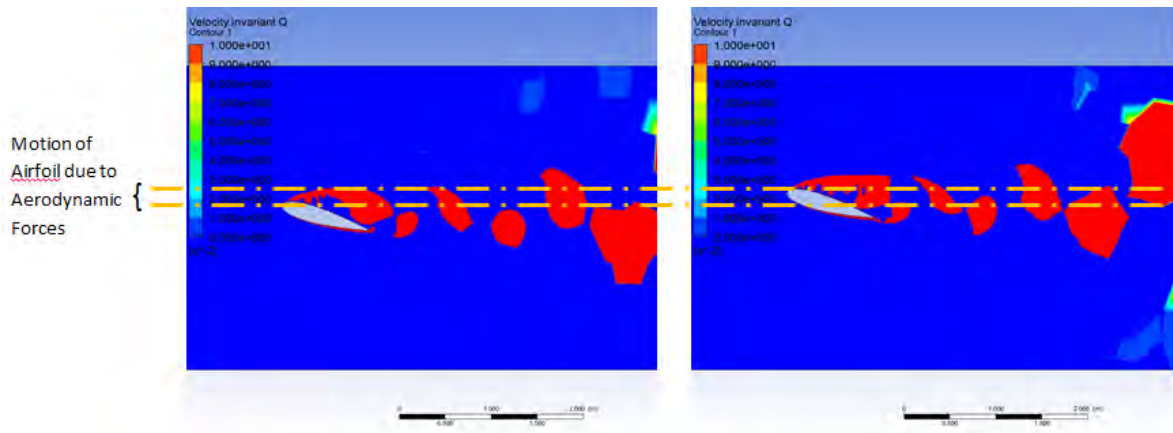


Figure 4.7 Motion of Airfoil in Y-Axis with RE100,000 and Stiffness 50K

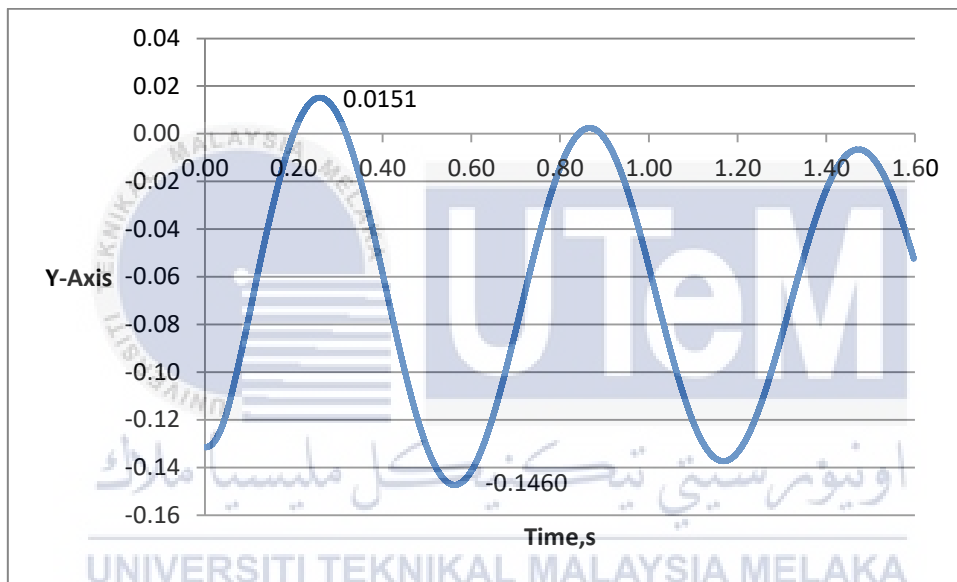


Figure 4.8 CG Motion of Airfoil System with Natural Frequency 1.59Hz

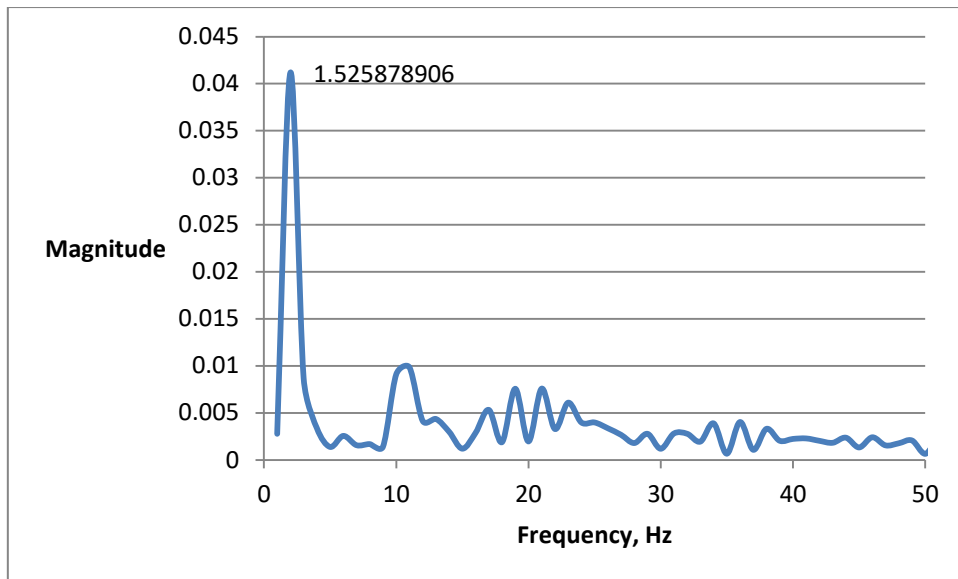


Figure 4.9 Frequency of CG Motion Natural Frequency 1.59

For a stiffness of 500,000 N/m and $Re_{10,000}$, the magnitude of airfoil movement along the y-axis is 0.25mm as shown in Figure 4.10 with a frequency of 4.88Hz shown in Figure 4.11.

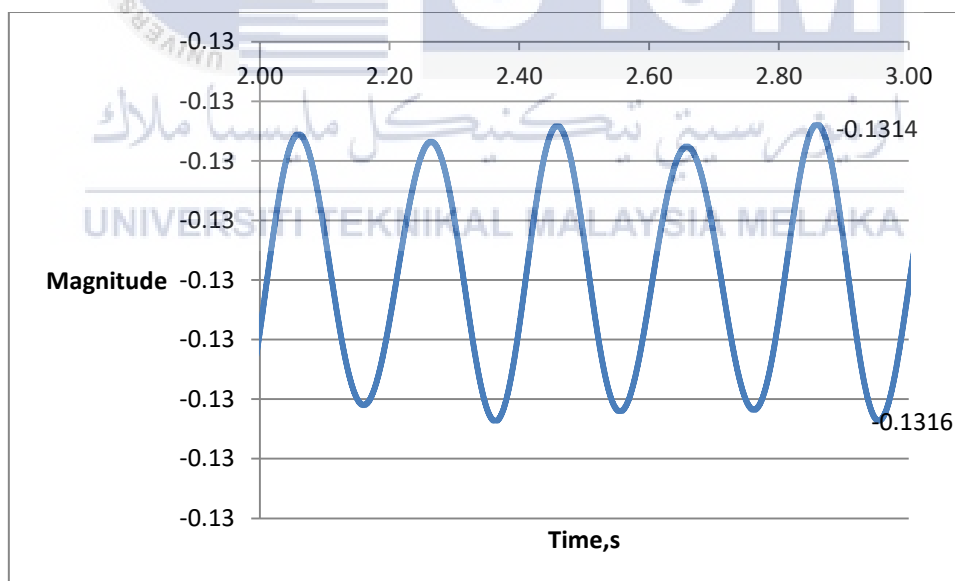


Figure 4.10 CG Motion of Airfoil System of Natural Frequency 5.03Hz

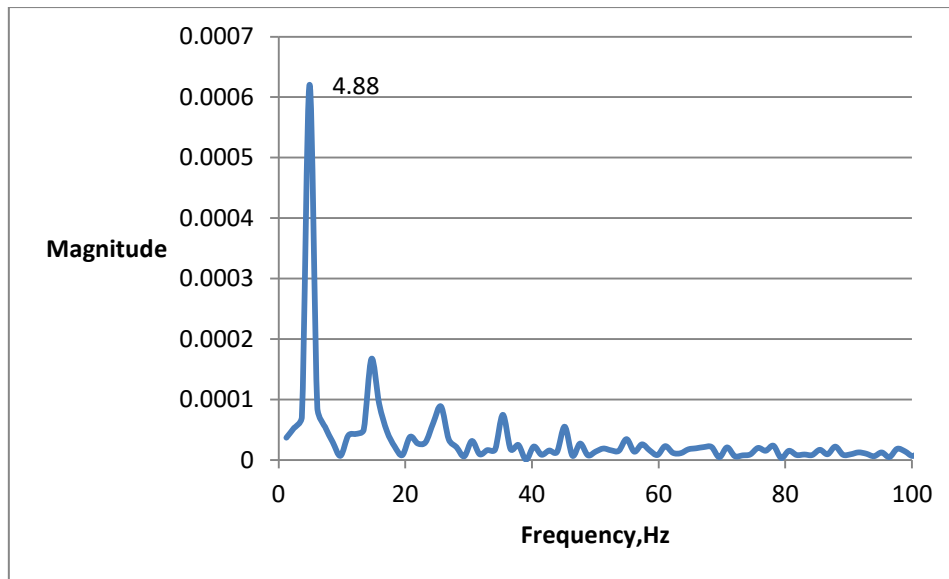


Figure 4.11 Frequency of CG Motion Natural Frequency 5.03Hz

Data from simulation of all system using $Re=100,000$ and $Re=10,000$ and its body response is summarized in Table 4.3. It shows that as the system stiffness increases, the magnitude of vibration decreases. A system of high stiffness is harder to move due to its inertia. System with lower stiffness is more prone to motion when subjected to aerodynamic forces. As vortex is being shed in a periodic manner behind the airfoil, the lift force will fluctuates hence causing the airfoil to moves along its y-axis in a periodic manner. When the system stiffness increases, the periodic motion of airfoil is restricted. The periodic motion changes to vibrational motion when the system is very stiff. This can be observed in the result of system with 49Million stiffness and $Re100,000$. The airfoil motion in this simulation only moves 10mm with a frequency of 48Hz. On the other hand, there is surprisingly no sudden enlargement in terms of magnitude for the movement of airfoil when the system natural frequency is in sync with the vortex shedding frequency of the airfoil. Resonance did not take place. For all cases, the natural frequency of system matches with the frequency of system motion when air is flowing pass the airfoil.

In simulation using $Re10,000$ some changes in magnitude of airfoil motion when compare to $Re=100,000$ is observed. For system stiffness of 50k, at $Re100,000$ the airfoil

moves 160mm but in $Re=10,000$ the airfoil only moves 1.71mm. There is a vast drop in airfoil movement. This is due to the aerodynamic force generated on the surface of the airfoil. As the flow reduces, the lift force generated on the surface of the airfoil reduces, this reduces the motion of the airfoil. As there is small aerodynamic forces acting on the surface of airfoil, the motion of airfoil in $Re=10,000$ is almost in vibrational mode. For system of 49Million stiffness, its vibrating frequency is 4775Hz which is very high. By using reducing Re to 10,000, it seems that for a system with lower Reynolds Number, the system Strouhal Number remains the same at 0.732.

Table 4.3 Data Comparison for System Stiffness and Body Motion

System			Re=100000		Re=10000	
Stiffness, 10^6	Natural Frequency	Reduced Frequency : f^*L/U	CG-Y Movement (Magnitude), mm	CG Motion Reduced Frequency : f^*L/U	CG-Y Movement (Magnitude), mm	CG Motion Reduced Frequency : f^*L/U
Fix	N/A	N/A	N/A	Na	Static	Static
0.05	1.59	0.02	160	0.0152	1.71	0.732
0.5	5.03	0.05	28	0.061	0.25	0.488
49	49.80	0.50	10	0.482	0.04	477.5
1,057	73.20	0.73	0.5	0.732	0.001	Static
50,000	1591.50	1.59	N/A	N/A	Static	Static

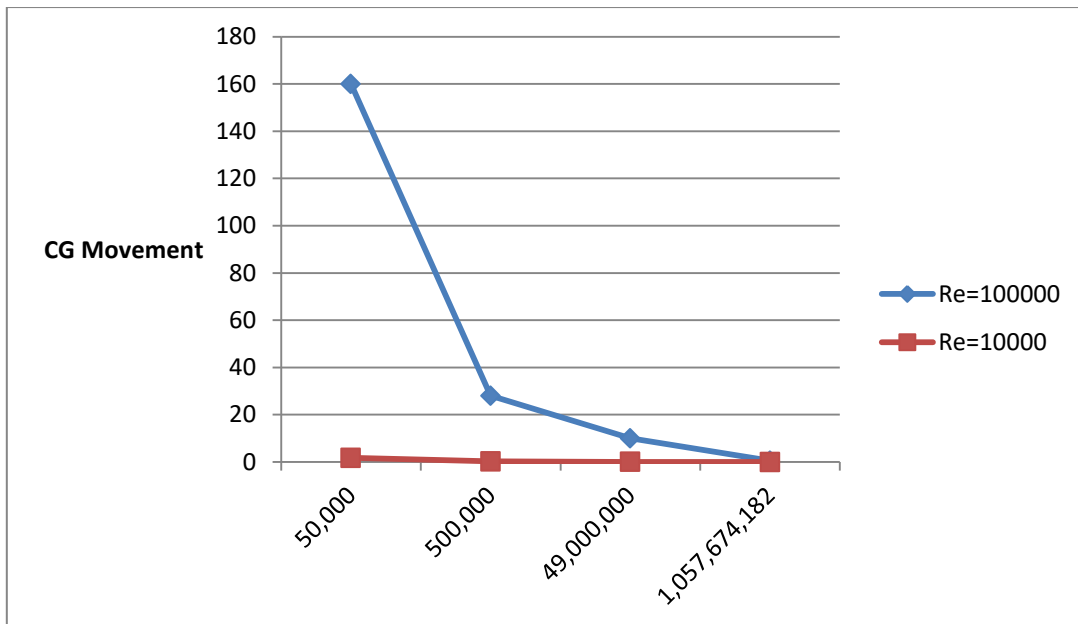


Figure 4.12 Graph of System Stiffness against Body Movement along Y-Axis

4.4 Stiffness vs Strouhal Number

For the simulation using a system with 50k N/m, Re100,000 and natural frequency of 1.59Hz, it is found that the lift force fluctuates at a range of 0.8-0.6. After FFT, it has a significant frequency of 73.21Hz. The lift data is found in Figure 4.12 and Figure 4.13.

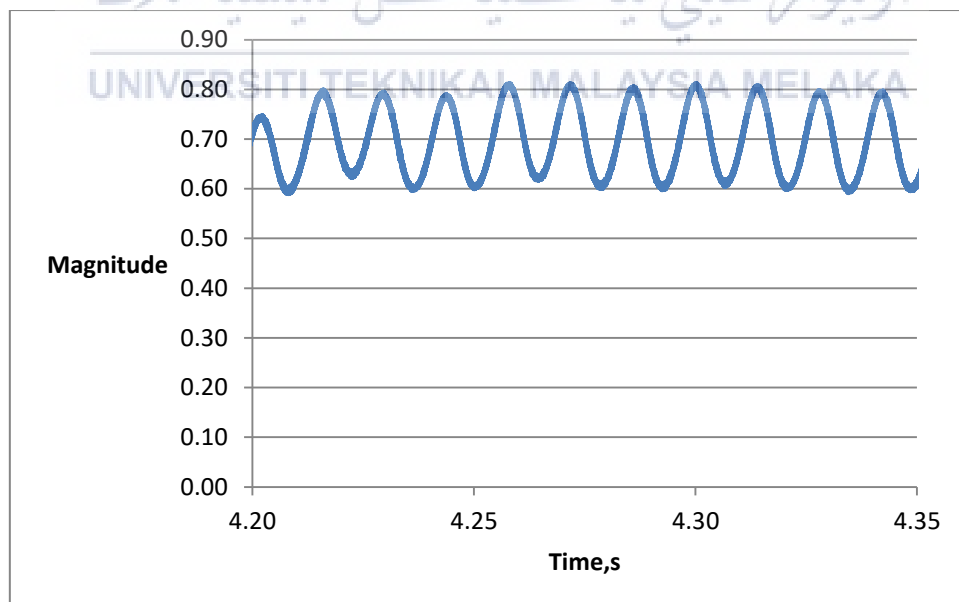


Figure 4.13 Lift Data NACA0018 with Natural Frequency 1.59Hz

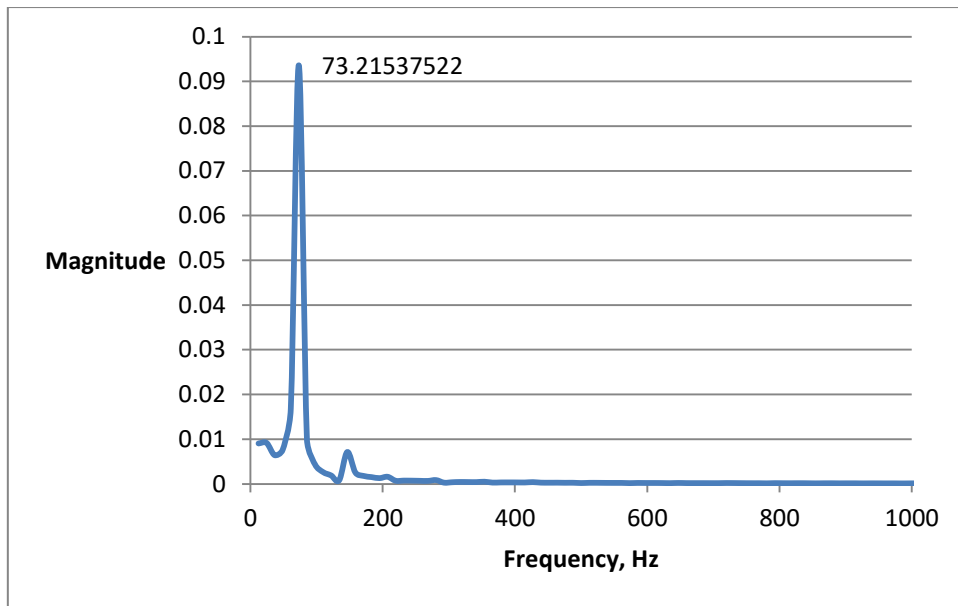


Figure 4.14 Frequency of Lift Data NACA0018 with Natural Frequency 1.59Hz

Another sets of experiments is carried out with a lower Reynolds Number to observe the Strouhal number changes due to system stiffness. Shown in Figure 4.14 is the periodic fluctuating lift force generated by the airfoil in an air flow of $Re=10,000$. FFT of the lift data gives the graph in Figure 4.15 which indicates significant peak at 7.32Hz and Strouhal Number of 0.732.

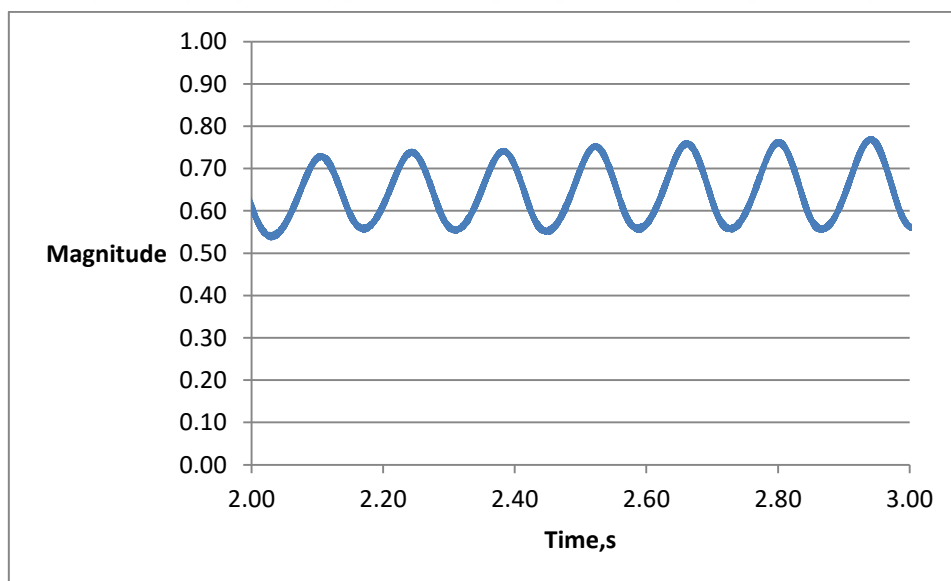


Figure 4.15 Lift Data NACA0018 with Natural Frequency 5.03Hz

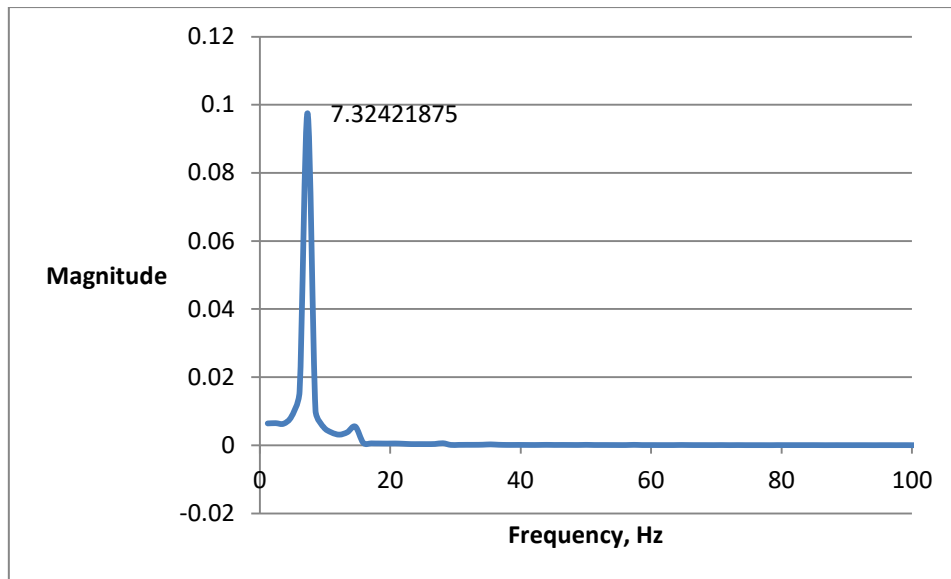


Figure 4.16 Frequency of Lift Data NACA0018 with Natural Frequency 5.03Hz

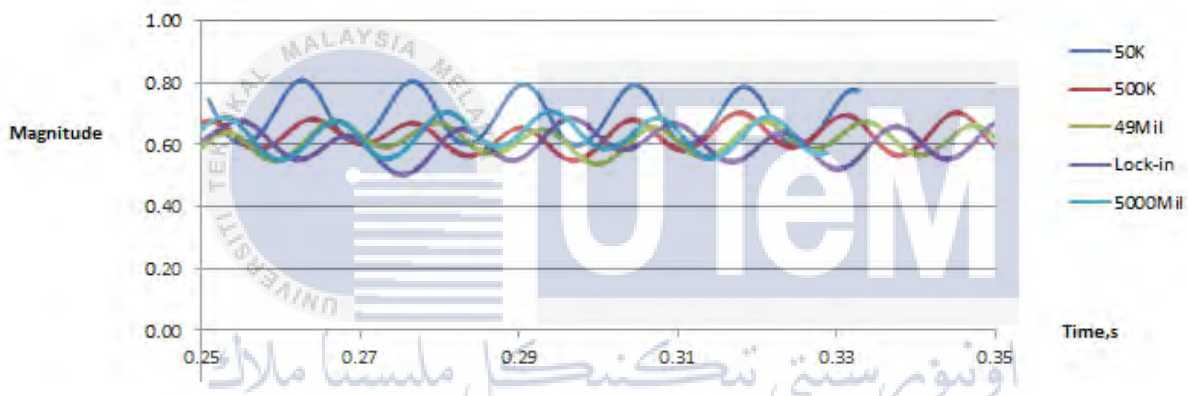


Figure 4.17 Lift Force Comparison for Different System Stiffness in Simulation Time

From Figure 4.16 it can be observe that the lift force seems to have the same phase of periodic motion. From simulation time of 0.26s – 0.32s every simulation cases experience 5 periods of lift force oscillation this explains the same vortex shedding frequency for each case. The only difference from all 5 cases here is the magnitude of lift force. System with less stiffness is able to develop higher magnitude of lift force and vice versa.

From the result obtained using Reynolds Number of 100,000, the system stiffness does not caused changes in vortex shedding frequency. This frequency remains the same as the frequency for a fixed airfoil. It seems that by including the rigid body motion during simulation will not cause changes in the system response due to fluid flow.

A point monitor is set up at the region of vortex shed as shown in Figure 4.17 to determine the vortex shed frequency. From the pressure fluctuation plot in Figure 4.18, there is periodic fluctuation of pressure force. Through Fourier Transform the pressure data, it is shown that the pressure fluctuating frequency is 73.2Hz for system stiffness of 1Million as shown in Figure 4.19. The Strouhal Number for this simulation at Re 100,000 is 0.732.



Figure 4.18 Monitor Point Setup To Collect Pressure Changes Due To Vortex Shedding

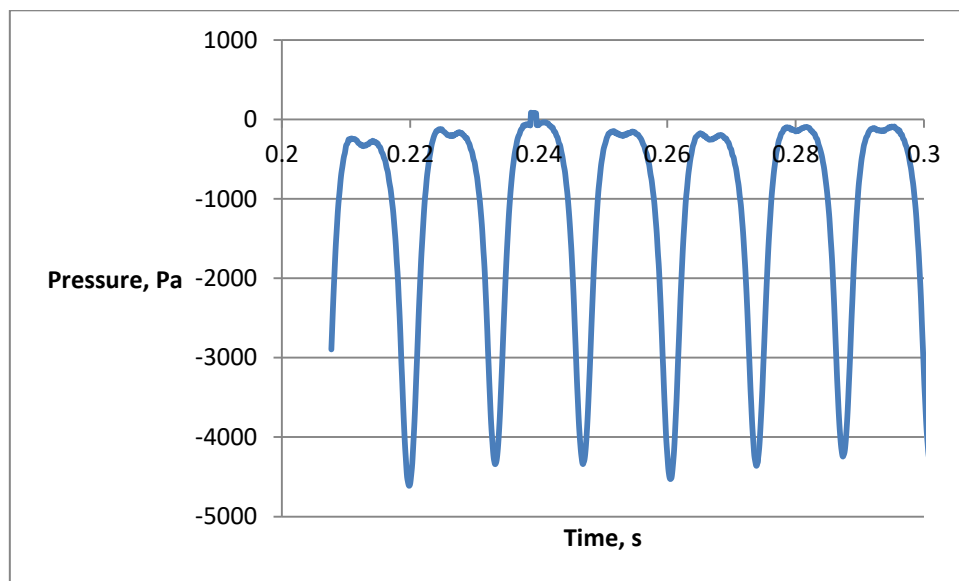


Figure 4.19 Pressure Fluctuation at Vortex Street

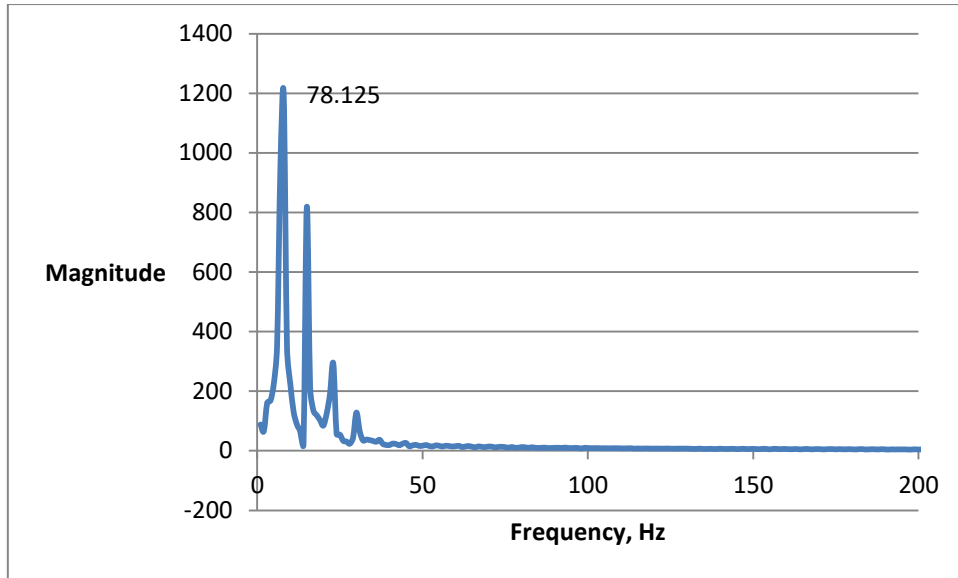


Figure 4.20 Frequency of Pressure Change

Table 4.4 Comparison System Stiffness with Strouhal Number

System			Re=100000		Re=10000	
Stiffness, 10^6	Natural Frequency	Reduced Frequency: f^*L/U	Vortex Shedding Frequency	Strouhal Number	Vortex Shedding Frequency	Strouhal Number
Fix	N/A	N/A	73.24219	0.732	7.324	0.732
0.05	1.59	0.02	73.2421	0.732	6.835	0.683
0.5	5.03	0.05	73.24219	0.732	7.3242	0.732
49	49.80	0.50	73.24219	0.732	7.3242	0.732
1,057	73.20	0.73	73.2	0.732	7.32	0.732
50,000	1591.50	1.59	73.24219	0.732	N/A	N/A

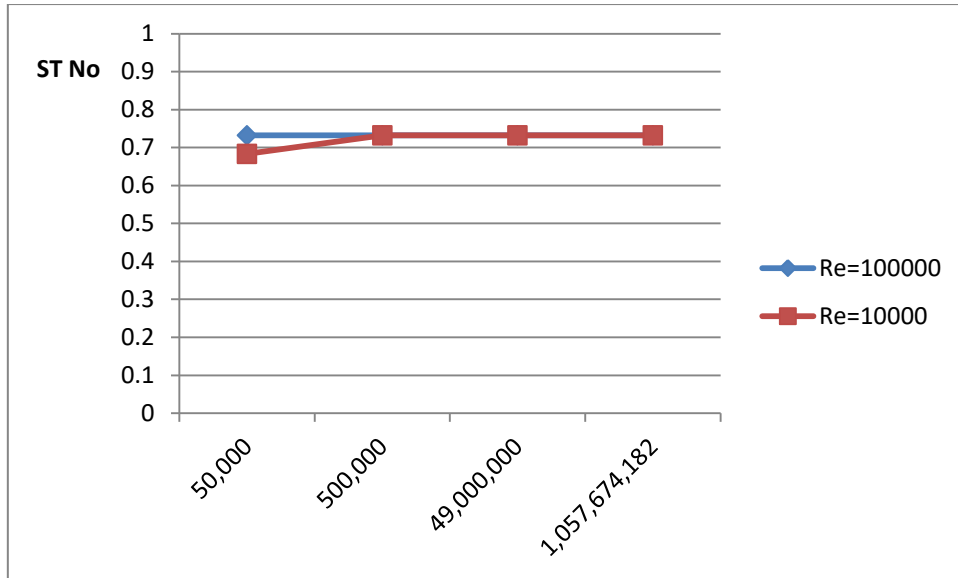


Figure 4.21 Graph of System Stiffness against Strouhal Number

Result at Table 4.4 shows the comparison of system stiffness and strouhal number obtained from simulation result of both Re 100,000 and Re 10,000. By plotting a graph shown in Figure 4.20 it seems that the change of Strouhal Number does not vary a lot. As stiffness increases, the Strouhal Number barely has any changes.

Table 4.5 Comparison Between Vortex Shed Frequency & Airfoil Motion Frequency for Re100,000

System Stiffness	System Reduced Natural Frequency	Lift Force Reduced Frequency	Strouhal Number	C.G Reduced Frequency
Fix Body	N/A	0.732	0.7320	Static
49 Million	0.50	0.732	0.7320	0.482
1000 Million	0.73	0.732	0.7810	0.732
50000 Million	1.59	0.732	0.7328	N/A

From Table 4.5 the motion of airfoil does has a C.G reduced frequency similar to the system natural frequency. This proves that the lift force periodic fluctuation of the airfoil is controlled by the vortex shedding frequency. Hence the Strouhal Number of system can be obtained from the frequency of lift force fluctuation.

4.5 Discussion on Non-Existence of Fluid Structure Interaction

From all the simulated result obtained, when the airfoil is fixed, Strouhal number obtained is 0.732. This value remains the same for cases with 1DOF fluid induced motion although the stiffness changes. The overall result is tabulated in Table 4.6. When Reynolds number is reduced to 10,000 the Strouhal number also did not change. Hence it can be seen that in this NACA0018 airfoil simulation with 1DOF carry out between the Reynolds Number of 100,000 to 10,000, the vortex shedding frequency of the airfoil remains the same despite changing the system stiffness. It shows that the body motion did not cause any changes in Strouhal number when compared to a fix airfoil.

Table 4.6 Overall Result Comparison

AIRFOIL NACA0018	STIFFNESS	STROUHALNUMBER
FIXED		0.732
ELASTICALLY MOUNTED 1DOF		-
RE 100,000	50,000	0.732
	500,000	0.732
	49,000,000	0.732
	1,057,674,182	0.732
	50,000,000,000	0.732
RE 10,000	50,000	0.683
	500,000	0.732
	49,000,000	0.732
	1,057,674,182	0.732
	50,000,000,000	N/A

The forced vibrational effect due to aerodynamic forces seems to only have minor effect on the system as the system is still vibrating in its natural frequency range. Besides the flow characteristic in this case is the Strouhal number remains the same throughout the simulation cases. This might be due to the large flow separation region behind the airfoil. When there is large flow separation, the fluid does not entirely intact to the body surface, the

aerodynamic forces acting on the body will be varied due to the separation. Wake characteristics might be an independent variable when flow separation is too large.



CHAPTER 5

CONCLUSION AND RECOMMENDATION

Airfoil when tilted to its stall angle will experience vortex shedding. This will cause the lift force generated on the upper and lower surface of airfoil to fluctuates. When the shedding of vortex is in a periodic manner, the lift force generated will also have the same periodic pattern.

From this experiment carried out, it shown that the motion of the rigid body will not affect the system response in a flowing fluid. For a fixed airfoil, the Strouhal number obtain is 0.732. The Strouhal number is similar for an airfoil where transverse motion is allowed and the stiffness of the system is manipulated. Even by changing the Reynolds Number of flowing fluid from 100,000 to 10,000, the Strouhal number is also 0.732.

Aerodynamic forces generated on the airfoil depend on the Reynolds Number of the flow. Larger Re produces higher aerodynamic forces which cause the motion of airfoil to increase. However in high Re flow, increasing system stiffness restrict its motion and the movement of airfoil will change to a vibrational motion. In conclusion, by integrating a 1DOF body motion into the simulation of airfoil will not affect the system response. This simulation shows body motion affected by fluid flow but no changes in wake characteristics when body motion is allowed. Therefore ignoring the body motion in this type of flow is acceptable.

Future research can focus of implementing 2 to 6 DOF into the simulation and investigate the impact of body motion on the system experiencing fluid flow. The system response due to body motion might vary due to the restriction given on the body. Besides that, the angle of attack of the airfoil can be change to reduce the separation region behind the

airfoil. When the flow is attach, the body motion might cause difference in flow induced effect on the system.



REFERENCES

- Abhiroop Jayanthi. (2008). Vortex Induced Vibration. *CHEST Journal*, 134(5), 1106.
<https://doi.org/10.1378/chest.08-1262>
- Ahzalilov, D. F. (1996). Airfoil design with external flow suction. *Fluid Dynamics*, 1(6), 46–818. <https://doi.org/10.1007/BF02030097>
- Breu, F., Guggenbichler, S., & Wollmann, J. (2008). CFD Study on Aerodynamic Effects of a Rear Wing Spoiler. *Vasa*, (December). Retrieved from <http://medcontent.metapress.com/index/A65RM03P4874243N.pdf>
- Chee Chew Wong. (2011). Naval Postgraduate. *EXPERIMENTAL STUDY OF FLUID STRUCTURE INTERACTION EFFECTS ON METAL PLATES UNDER FULLY DEVELOPED LAMINAR FLOW*, (December), 87.
- Derakhshandeh, J. F., Arjomandi, M., Dally, B., & Cazzolato, B. (2016). Flow-induced vibration of an elastically mounted airfoil under the influence of the wake of a circular cylinder. *Experimental Thermal and Fluid Science*, 74, 58–72.
<https://doi.org/10.1016/j.expthermflusci.2015.12.003>
- Elsayed, O. A., Omar, A. A., Asrar, W., & Kwon, K. (2011). Effect of differential spoiler settings (DSS) on the wake vortices of a wing at high-lift-configuration (HLC). *Aerospace Science and Technology*, 15(7), 555–566.
<https://doi.org/10.1016/j.ast.2010.11.001>
- Gharib, M. R. (1999). Vortex Induced Vibration .Pdf.
- Hansen, S. O. (2007). Vortex-induced vibrations of structures. *Structural Engineers World Congress*, 2–7.
- Hansen, S. O., Srouji, R. G., Isaksen, B., Berntsen, K., Ole, S., & Aps, H. (2015). Vortex-

- induced vibrations of streamlined single box girder bridge decks, 1–14.
- Hessenthaler, A., Gaddum, N. R., Holub, O., Sinkus, R., Röhrle, O., & Nordsletten, D. A. (2016). Experiment for validation of fluid-structure interaction models and algorithms. *International Journal for Numerical Methods in Biomedical Engineering*, 1–30. <https://doi.org/10.1002/cnm.2848>
- Hetawal, S., Gophane, M., Ajay, B. K., & Mukkamala, Y. (2014). Aerodynamic study of formula SAE car. *Procedia Engineering*, 97, 1198–1207. <https://doi.org/10.1016/j.proeng.2014.12.398>
- Holmes, S. (2008). Race Car Aerodynamics. *E. Nz Magazine: The Magazine of Technical ...*. Retrieved from <http://search.informit.com.au/fullText;dn=008702579191600;res=IELENG>
- Kieffer, W., Moujaes, S., & Armbya, N. (2006). CFD study of section characteristics of Formula Mazda race car wings. *Mathematical and Computer Modelling*, 43(11–12), 1275–1287. <https://doi.org/10.1016/j.mcm.2005.03.011>
- Kuya, Y., Takeda, K., Zhang, X., Beeton, S., & Pandaleon, T. (2009). Flow separation control on a race car wing with vortex generators in ground effect. *Journal of Fluids Engineering, Transactions of the ASME*, 131(12), 1211031–1211039. <https://doi.org/10.1115/1.4000420>
- Lienhard, J. H. (1966). Synopsis of lift, drag, and vortex frequency data for rigid circular cylinders. *Bulletin 300*.
- Lienhart, H., & Pereira Gomes, J. (2006). Experimental study on a two-dimensional fluid-structure interaction reference test case. *Proceedings of the European Conference on Computational Fluid Dynamics*. Retrieved from <http://proceedings.fyper.com/eccomascfd2006/documents/529.pdf>
- Meederira, P. B. (2014). Aerodynamic development of a IUPUI Formula SAE specification

- car with Computational Fluid Dynamics(CFD) analysis Ponnappa Bheemaiah Meederira, Indiana- University Purdue- University. Indianapolis.
- Mertins, R., Elsholz, E., Barakat, S., & Colak, B. (2005). Dreidimensionale reibungsfreie Strömungsuntersuchungen an Flügel-Rumpf-Querruder-Spoiler Konfigurationen. *Aerospace Science and Technology*, 9(6), 476–484. <https://doi.org/10.1016/j.ast.2005.06.003>
- Mysa, R. C., Kaboudian, A., & Jaiman, R. K. (2016). On the origin of wake-induced vibration in two tandem circular cylinders at low Reynolds number. *Journal of Fluids and Structures*, 61, 76–98. <https://doi.org/10.1016/j.jfluidstructs.2015.11.004>
- Nakano, T., Fujisawa, N., Oguma, Y., Takagi, Y., & Lee, S. (2007). Experimental study on flow and noise characteristics of NACA0018 airfoil. *Journal of Wind Engineering and Industrial Aerodynamics*, 95(7), 511–531. <https://doi.org/10.1016/j.jweia.2006.11.002>
- Nguyen, V.-T., & Nguyen, H. H. (2016). Detached eddy simulations of flow induced vibrations of circular cylinders at high Reynolds numbers. *Journal of Fluids and Structures*, 63, 103–119. <https://doi.org/10.1016/j.jfluidstructs.2016.02.004>
- Olsson, S. (2014). Fluid structure interaction analysis on the aerodynamic performance of underbody panels.
- Pantazopoulos, & Pantazopoulos, M. S. (1994). Vortex-induced vibration parameters: Critical review. *1994 OMAE- Volume 1. Offshore Technology*.
- Pellegrino, A., & Meskell, C. (2013). Vortex shedding for a pitching wind turbine blade section at high angles of attack. *Journal of Wind Engineering and Industrial Aerodynamics*, (121), 131–137. Retrieved from <http://dx.doi.org/10.1016/j.jweia.2013.08.002>
- Shan, H., Jiang, L., & Liu, C. (2005). Direct numerical simulation of flow separation around a NACA 0012 airfoil. *Computers & Fluids*, 34(9), 1096–1114.

<https://doi.org/10.1016/j.compfluid.2004.09.003>

- Singh, S. P., & Mittal, S. (2005). Vortex-induced oscillations at low Reynolds numbers: Hysteresis and vortex-shedding modes. *Journal of Fluids and Structures*, 20(8), 1085–1104. <https://doi.org/10.1016/j.jfluidstructs.2005.05.011>
- Tsai, C. H., Fu, L. M., Tai, C. H., Huang, Y. L., & Leong, J. C. (2009). Computational aeroacoustic analysis of a passenger car with a rear spoiler. *Applied Mathematical Modelling*, 33(9), 3661–3673. <https://doi.org/10.1016/j.apm.2008.12.004>
- Vinuesa, R., Hosseini, S. M., Hanifi, A., Henningson, D. S., & Schlatter, P. (2016). Direct numerical simulation of the flow around a wing section using high-order parallel spectral methods. *International Symposium on Turbulence and Shear Flow Phenomena*, 0(JANUARY), 1–6. <https://doi.org/10.1016/j.ijheatfluidflow.2016.02.001>
- Wang, Y. N., Tseng, C. Y., Huang, Y. L., & Leong, J. C. (2010). Investigation of 2004 Ferrari Formula One race car wing effects. *3CA 2010 - 2010 International Symposium on Computer, Communication, Control and Automation*, 1, 85–88. <https://doi.org/10.1109/3CA.2010.5533726>
- Williamson, C. H. K., & Govardhan, R. (2004). Vortex-Induced Vibrations. *Annual Review of Fluid Mechanics*, 36(1), 413–455. <https://doi.org/10.1146/annurev.fluid.36.050802.122128>
- Yarusevych, S., Sullivan, P. E., & Kawall, J. G. (2009). On vortex shedding from an airfoil in low-Reynolds-number flows. *Journal of Fluid Mechanics*, 632, 245. <https://doi.org/10.1017/S0022112009007058>
- Zahari, M. A., & Dol, S. S. (2014). Application of Vortex Induced Vibration Energy Generation Technologies to the Offshore Oil and Gas Platform : The Preliminary Study, 8(7), 1317–1320.
- Zhang, G. Q., & Ji, L. C. (2016). Investigation of two degrees of freedom on vortex-induced

vibration under the wake interference of an oscillating airfoil. *Acta Astronautica*,
(October). <https://doi.org/10.1016/j.actaastro.2016.10.041>



